INSTYTUT FIZYKI JĄDROWEJ
INSTITUTE OF NUCLEAR PHYSICS
ИНСТИТУТ ЯДЕРНОЙ ФИЗИКИ

KRAKÓW

INP – RAPORT No 1199/PL

STUDY OF HIGH ANGULAR MOMENTUM PHENOMENA IN ROTATING NUCLEI

WŁADYSŁAW WALUŚ

KRAKÓW 1982

STUDY OF HIGH ANGULAR MOMENTUM PHENOMENA IN ROTATING NUCLEI

WYSOKOSPINOWE EFEKTY W SZYBKO OBRACAJĄCYCH SIĘ JĄDRACH

ИССЛЕДОВАНИЕ СВОЙСТВ ВЫСОКОСПИНОВЫХ СОСТОЯНИЙ В БЫСТРО ВРАЩАЮЩИХСЯ ЯДРАХ

Władysław Waluś

Institute of Physics, Jagellonian University,
30-059 Cracow, Reymonta 4

October 1982

NAKŁADEM INSTYTUTU FIZYKI JĄDROWEJ W KRAKOWIE
UL. RADZIKOWSKIEGO 152

Kopię kserograficzną, druk i oprawę wykonano w IFJ Kraków

Wydanie I Zam. 168/82 Nakład 120 egz.

Abstract

Information about rotational bands of deformed Yb nuclei as obtained through in-beam spectroscopic studies are discussed. Routhians and alignments have been extracted from the experimental data. Experimental single-quasineutron routhians have been used to construct two- and three-quasineutron routhians. Residual interaction between excited quasiparticles are obtained from a comparison of the excitation energies of multiple-quasiparticle states constructed from single-quasiparticle states with experimental excitation energies of multiple-quasiparticle states. An odd--even neutron-number dependence of the alignment frequency of the first pair of $i_{13/2}$ quasineutron in rare-earth nuclei is presented. This effect is explained by a reduction of the neutron pairing--correlation parameter, Δ_n, for odd-N systems as compared to seniority-zero configurations in even-N nuclei. The signature dependence of the interband-intraband branching ratios as well as of the interband M1/E2 mixing ratios is discussed, and compared to the signature dependence of $B(M1)$ transition rates recently suggested by Hamamoto.

Przedstawiono analizę własności poziomów wysokospinowych dla izotopów Yb z obszaru $160 \leqslant A \leqslant 168$. Na podstawie ustalonych schematów poziomów energetycznych otrzymano kwaziczątkowe energie (routhiany) w układzie rotujących współrzędnych. Wyznaczono uszeregowanie spinów dla obserwowanych rotacyjnych pasm. Skonstruowano routhiany dwu- i trój-kwaziczątkowe ze znanych doświadczalnie routhianów jedno-kwaziczątkowych. Porównując routhiany tak otrzymane z routhianami eksperymentalnie znanych pasm wielo-kwaziczątkowych wyznaczono resztkowe oddziaływanie pomiędzy wzbudzonymi kwaziczątkami. Przedstawiono systematykę częstości kątowej $\hbar\omega_c$ przy której następuje uszeregowanie pierwszej pary neutronowej z powłoki $i_{13/2}$ dla jąder z obszaru ziem rzadkich o $90 \leqslant N \leqslant 98$. Stwierdzono systematyczne obniżanie $\hbar\omega_c$ dla jąder o nieparzystej liczbie neutronowej N. Efekt ten tłumaczy się redukcją neutrono-

wego pairingu, Δ_n, w jądrach o nieparzystym N w porównaniu do jąder o parzystym N. Przedstawiono doświadczalne potwierdzenie silnej zależności B(M1) od częstości obrotu $\hbar\omega$ i sygnatury.

Приведён анализ свойств высокоспиновых состояний в ядрах Yb из области $160 \leq A \leq 168$. На основе экспериментальных ротационных уровней найдено квазичастичные энергии во вращающейся системе координат. Определено выстраивания углового момента для разных состояний ротационных полос. Вычислены двух- и трёхквазичастичные энергии во вращающейся системе координат из экспериментально известных одноквазичаотичных энергий. Приведена зависимоть ротационной частоты $\hbar\omega_c$, при которой наступает разрыв первой нейтронной пары из полосы $i_{13/2}$ от числа нейтронов в области $90 < N < 98$. Замечено систематическое уменьшение $\hbar\omega_c$ для ядер с нечётным числом нейтронов. Представлено экспериментальное подтверждение сильной зависимости B(M1) от ротационной частоты и сигнатуры.

Contents

1. Introduction 7
2. Experimental techniques 12
3. The cranked shell-model 19
4. Transformation of the decay-scheme information to e′ versus $\hbar\omega$ representation 23
5. The spectrum of single-quasineutron states in odd-A Yb isotopes 29
6. Construction of multiple-quasineutron states from the spectrum of single-quasineutron states 32
7. Band-crossing systematics in Yb nuclei 38
8. Comparison with cranked shell-model calculations 43
9. Evidence for strong rotational effects on M1 transitions 52
10. Summary 55
11. References 58

1. Introduction

In heavy ion collisions, it is possible to produce compound nuclei with angular momenta which may reach the maximum values that can be accomodated by rotating nuclei. A limit for studying high angular momentum phenomena is therefore provided by the fission instability of compound nuclei caused by rotation. With increasing angular momentum, one arrives at a critical value I_{max} at which the compound nucleus is no longer stable with respect to fission. The value of I_{max}, obtained from liquid drop model, as a function of nuclear mass number is shown in fig. 1. Compound nuclei lying below the curve where the fission barrier equals 8 MeV /B_f=8 MeV/ decay by particle evaporation leading to so-called evaporation residues. It is seen in fig. 1 that the curve labelled B_f=8 MeV reaches a maximum of about I=80ħ around A=140, while the curve B_f=0 MeV reaches I≈100ħ around A=130.

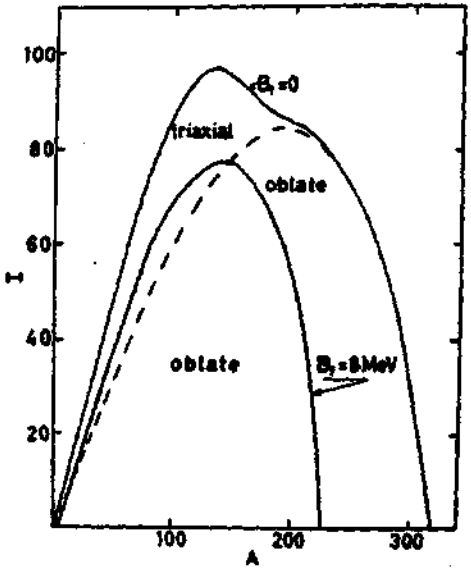

Fig. 1. Fission stability of rotating liquid drop. The figure is taken from the theoretical analysis of reference 1, and shows the value of the angular momentum that can be accomodated by the beta-stable nuclei as a function of the mass number A. The stable shape of the nucleus is oblate below the dashed line and triaxial between the dashed and solid line

The several evaporated particles /mostly neutrons/ carry away only a small part of the total angular momentum, but much of energy and thus most of the angular momentum remains in the evaporation residues. The rest of the excitation energy and angular momentum is released through gamma decay. The γ - ray decay becomes competative with particle emission near the γ - ray "entry line". This line is defined in the energy versus angular momentum plane as the centroid of states prior to the γ - decay, and roughly coincides with the line of equal probability for γ - ray and neutron emission. The deexcitation of the nucleus is schematically shown in fig. 2. The entry line is expected to be parallel to the line of states of the lowest possible energy at a certain angular momentu [2]. These states are called the yrast states. In the angular momentum versus energy plane, the yrast line forms the boundary between the physically possible states and physically impossible states. In other words, there are no states below the yrast line.

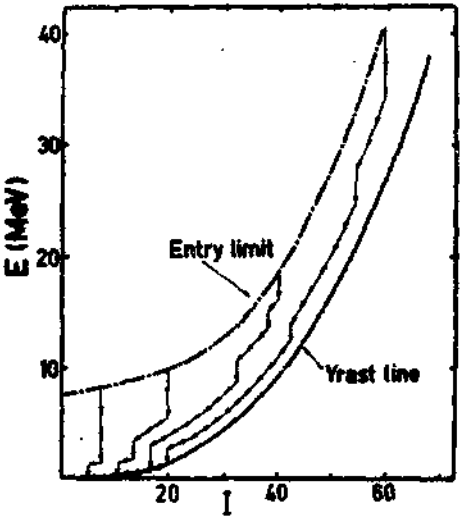

Fig. 2. A typical picture of γ-ray deexcitation pathways to the ground state. The statistical transitions are the vertical arrows which lower the temperature of the system, whereas the yrast-like transitions are roughly parallel to the yrast line and remove the angular momentum of the system.

The nucleus can decay vertically toward the yrast line by statistical transitions that decrease the excitation energy of the nucleus and only a little angular momentum. It can decay also by collective E2 transitions that form bands parallel to the yrast line and carry off angular momentum as well as energy. There are so many possible pathways that the γ-transitions form a continuous γ-ray spectrum. No single transition has enough intensity to be seen in the spectrum. When the nucleus deexcites close to the yrast line, there are much less pathways and enough population goes through individual transitions to make them stand out in the spectrum as resolved lines. This happens between spins of 10$\hbar$ to 40$\hbar$ depending on the type of nucleus, and the observed lines can correspond to either collective or noncollective transitions, according to the nature of the yrast states.

The statistical transitions do not depend very much on the nuclear structure, but the existence of collective rotational transitions does. In particular, it requires rotation around an axis other than the symmetry axis. For a prolate nucleus /and a triaxial nucleus favouring prolate shape/ rotating around an axis perpendicular to the symmetry axis, the transitions in rotational bands are strongly enhanced and prefere the decay roughly parallel to the yrast line. Thus, they lead to low spins before sufficient cooling takes place to allow observation of the discrete lines / 30$\hbar$/. On the other hand, oblate nuclei /or triaxial nuloi of dominantly oblate shape/ rotating around their symmetry axis have no collective transitions /or strongly suppressed/, and so th deexcite more steeply into the yrast line. It is reached at a hig her spin and, since in this case the yrast line is irregular bein composed of single-particle states, not only are discrete states of higher spin observable, but some may be long-lived enough to became isomers, so called the yrast traps [3].

In the yrast region the nucleus is cold in the sense that almost all the excitation energy of the nucleus is tied up in generating the angular momentum. Therefore, the structure in the yrast region should be described with simple excitation modes This leads to the concept of "yrast spectroscopy" which extends

the spectroscopy of low lying states to the whole yrast region [4].

In the past decade, many new features of nuclei have been found through detailed experimental investigations of the yrast region. One of the major discoveries, was the observation of the backbending phenomenon in many deformed nuclei.

The backbending phenomenon, is now understood to result from the crossing of bands of different degrees of rotational alignment [5]. In the even-even Z=64 - 72 nuclei the backbending feature of the yrast bands has been well studied and it has been found that the s-band /Stockholm or super/ which crosses the ground state band at I=12-16 has additional angular momentum that can be attributed to the alignment of a pair of $i_{13/2}$ neutrons. But, band crossings and backbendings should not be a feature characteristic of the yrast band only. Near the yrast line, there should exist many 2 q.p. or 1 q.p. /in odd nuclei/ bands, which may also experience backbending or upbending due to the alignment of a pair of high-j quasiparticles near the Fermi surface /$i_{13/2}$ neutrons or $h_{11/2}$ protons in the case of rare-earth nuclei/. A study of not only the yrast band but also of other bands is thus imperative for a proper understanding of the influence of rotation on quasiparticles near the Fermi surface.

The present article is based on the systematic studies of band structure in the Yb nuclei. It concentrates on the problems how to obtain spectroscopic information from such studies and summarizes some spectroscopic information. In those studies the cranked shell model and the particle-rotor model were used as the theoretical approaches. Both models invoke the idea of a statically deformed field that rotates with respect to the laboratory reference frame. In the particle-rotor model the majority of the nucleons are represented by a rotor having only rotational degrees of freedom whereas the degrees of freedom of one or a few remaining nucleons are treated explicitly [6,7,8]. The particle-rotor hamiltonian refers to the laboratory system and properties of states are calculated as functions of angular momentum. The cranking model first used by Inglis [9], deals with the motion of the nucleons in a rotating reference frame. From the response of the nu-

cleons to this rotation, all nuclear properties can be explicitly expressed as functions of the rotational frequency. The interpretation of the band structure and band crossings according to the idea of Bohr and Mottelson [4] provides us with means to compare the experimental results with a microscopic theory and to extract quantities like the crossing frequency and the aligned angular momentum from the experimental data. These methods have been further developed by Bengtsson and Frauendorf [10].

2. Experimental techniques.

The decay sequences of deformed nuclei are composed of cascades along a series of rotational bands, each based on a definite intrinsic configuration. It is illustrated in fig. 3 where the level scheme of ^{165}Yb is presented. The methods of in-beam γ-ray

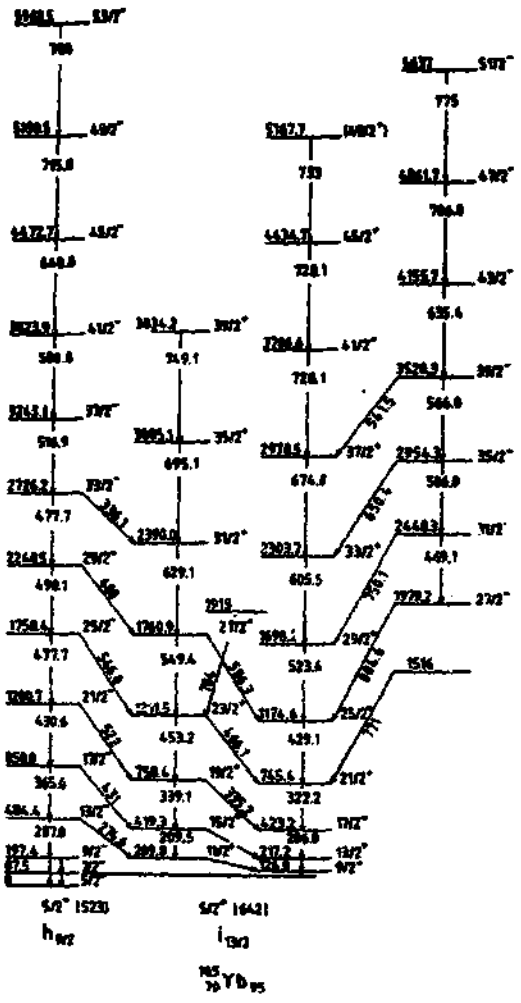

Fig. 3. Level scheme of ^{165}Yb, showing states populated in the ^{152}Sm /^{17}O,4n/ ^{165}Yb reaction at 80 MeV of bombarding energy of ^{17}O.

spectroscopy used for establishing such bands are based on the studies of angular distributions, $\gamma - \gamma$ coincidences, conversion electron coefficients, excitation functions and life-times of excited states. Such studies on which this paper is based were carried out at the N.B.I. tandem accelerator using 80 - 84 MeV beams of $^{16,17,18}O$ and 60 - 65 MeV beams of ^{12}C on $^{149,152,154}Sm$ targets [11,12,13,14,15].

In the study of rotational bands up to high spins it is often difficult to resolve the highest transitions because of a large number of lines in the spectrum. The quality of the recorded data can, however, be considerably improved by favouring the registration of events belonging to high-multiplicity cascades. This can be done by means of a multiplicity filter or a sum-energy filter methods.

In the multiplicity filter method, several individual NaJ/Tl/ counters are used in addition to high-resolution Ge/Li/ detectors employed for energy registration. The technique consists in requiring the detection of at least three γ-rays in the multi-counter system, within a pre-set coincidence overlap time before accepting any event. Therefore, the registration of transitions belonging to high-multiplicity cascades is strongly enhanced. Since the multiplicity of the rotational cascades depends mainly on the angular momentum input [16], the multiplicity requirement improves greatly the selection of a specific xn-channel and the exclusion of low-multiplicity or background events. Such selection can be also done by using of one or more NaJ/Tl/ counters with a large total solid angle, as a total γ-ray energy filter [17]. A Ge/Li/-event is thus only accepted if there is a simultaneous /within the resolving time/ registration of the total energy exceeding a pre-set threshold. Since the binding energy of the neutron is larger than the kinetic evaporation energy of the emitted neutrons, one expects a small overlap between the xn-channels on the energy axis and a good channel selection in the total energy of the γ-ray cascade measured in the sum spectrometer. It is therefore possible to discriminate the resulting events off the events from unwanted reactions. This can be seen in fig. 4 where the Ge/Li/ γ-ray spectra

from the ^{144}Sm /^{12}C,xn/ $^{156-x}Er$ reaction are presented. In the ^{144}Sm /^{12}C,xn/ $^{156-x}Er$ reaction, there is less energy available for γ-radiation after the evaporation of three neutrons than after the evaporation of two nautrons.

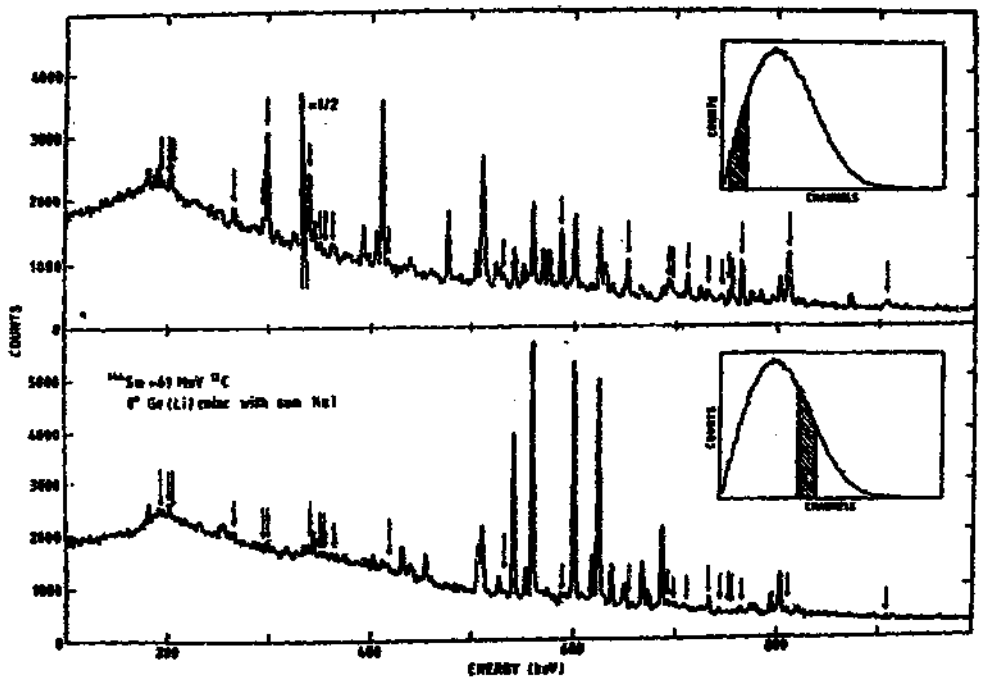

Fig. 4. The Ge/Li/ γ-ray spectra obtained with a gate placed on the low-energy part /upper spectrum/ and on the high-energy part /lower spectrum/ of the sum-spectrum recorded in a NaJ/Tl/ detector subtending a solid angle of 70% of 4π. The transitions of ^{153}Er are marked with arrows.

Therefore in the low-energy part of the spectrum recorded by the sum spectrometer, the transitions of ^{153}Er are much stronger than in the high energy part, which is dominated by the transitions of ^{154}Er. The γ-ray intensities in the spectrum obtained with the

Ge/Li/-detectors in the coincidence with the low-energy part of the sum spectrum, are an order of magnitude larger for the transitions of ^{153}Er than for the transitions of ^{154}Er.

The analysis of energy-energy-time coincidences between the emitted nuclear radiation gives the most important information necessary for construction of the nuclear level schemes. In a typical coincidence experiment two Ge/Li/ detectors are used. The low coincidence counting rate obtainable with such a two-detector system is not suited for the study of weakly populated bands, for which high statistics is very important. The use of many detectors can solve this problem. For example the use of four detectors would increase the coincidence counting rate by a factor of about 6 when compared to a two-detector system. In the coincidence experiment on ^{166}Yb, 4 Ge/Li/ detectors were used. The gains of the detectors were matched to be equal so the resultant spectra could be added. Furthermore, 4 NaJ/Tl/ detectors served as multiplicity filter. Only those events were recorded in which at least three detectors /of which at least two were Ge/Li/ detectors/ were triggered. The coincidence counting rate was approximately 1000 counts/sec. using a 1 particle nA beam of 80 MeV ^{16}O on a 1.5 mg/cm^2 ^{154}Sm target. A similar set-up, in which one of the Ge/Li/ detectors was replaced by a planar Ge/Li/ detector was used for the coincidence experiment on ^{167}Yb. These set-ups favour high-multiplicity events and virtually eliminate all events duo to radioactivity. This is important when studing weak transitions as the product nuclei are usually highly radioactive.

The coincidence experiments on ^{163,164,165}Yb were perforued with a set-up consisting of 5 Ge/Li/ detectors in Compton-suppresion shields. The arrangement of this set-up is schematically shown in fig. 5. Four of the Compton-suppresion shields were 8 x 10 inch NaJ/Tl/ crystals, the fifth was a smaller NaJ/Tl/ crystal. This set-up reduced the background drastically, it permitted an easy and a positive identification of weak transitions in the gated spectra and it made possible to gate on weak transitions. The improved quality of the coincidence data is significant which can be seen in fig. 6, where the comparison of gated suppressed

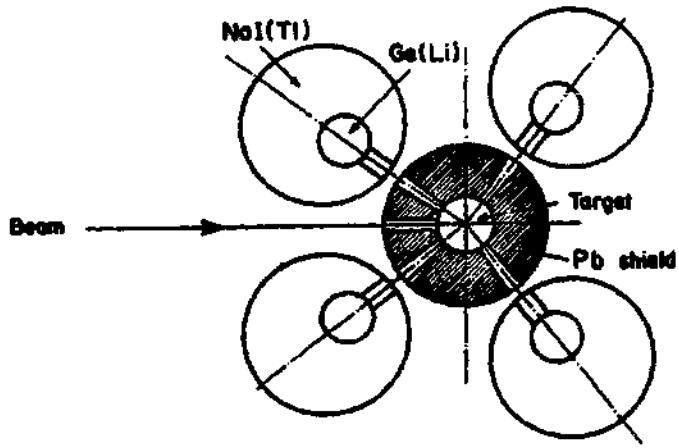

Fig. 5. Schematic side view of the arrangement of the array of four anticompton spectrometers. A fifth anticompton spectrometer is located in the horizontal plane at 90° to the beam direction.

and nonsuppressed spectra is presented. The suppresion of the Compton events resulted also in an almost 5-fold reduction of the coincidence data to be handled. Furthermore, the use of 5 detectors enabled to run the coincidance experiment with a reasonable counting rate. A 3 partiole nA beam of 80 MeV ^{17}O on a 2 5 mg/cm^2 target of ^{152}Sm resulted in about 400 Compton, suppressed coincidences /sec

In order to study low-energy transitions 20 keV $< E_\gamma <$ 300 keV in ^{163}Yb, a X-γ- time coincidence experiment was performed using a set-up consisting of one Ge intrinsio detector sensitive to the X-ray and four big Ge/Li/ detectors with matched gain amplifiers. A multiplicity filter of four NaJ/Tl/ detectors was also used. In this experiment the TAC was started by the pulse corresponding to the detection of an event in the X-ray detector and stopped by delayed pulse from the γ- detectors.

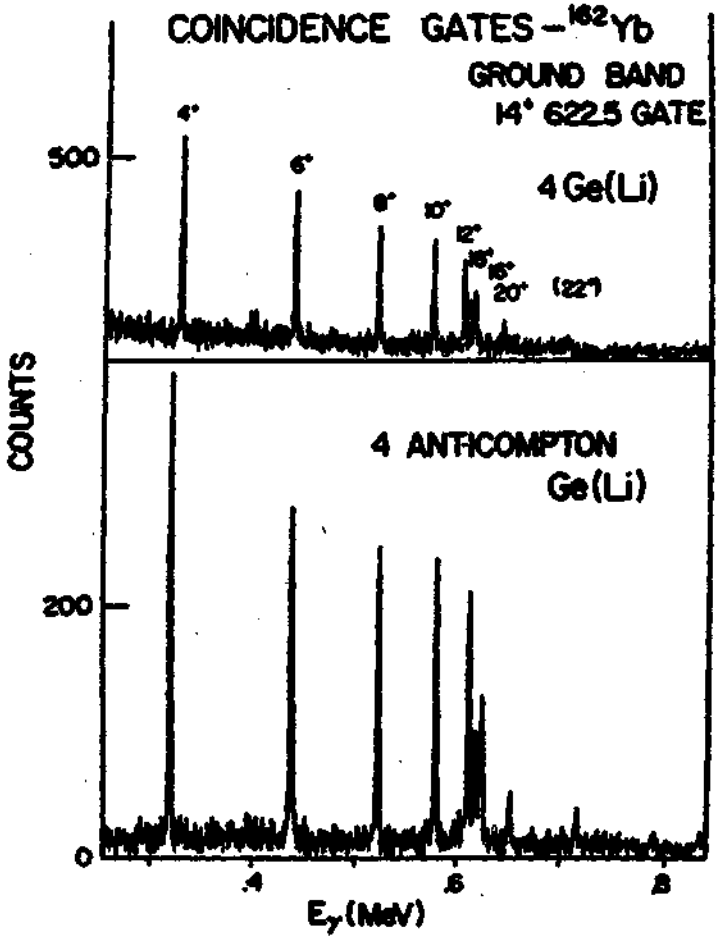

Fig. 6. Comparison of coincidence γ-ray spectra for ^{162}Yb obtained with Compton-suppressed Ge/Li/ detectors /bottom/ and unsuppressed Ge/Li/ detectors /top/. Note the improved peak to background ratio for the spectra obtained with Compton-suppressed Ge/Li/'s.

For the study of the angular distribution of the γ-rays, two sets of single γ-ray spectra were measured simultaneously at 5 different angles between 0° and 90°. A single Ge/Li/ detector and a Compton-suppressed Ge/Li/ detector were used for the two sets respectively. These two detectors were mounted on a common turntable at right angle to each other. A third detector placed below the target served as a monitor detector. The beam was stopped by a 0.3 mm lead foil inside the target chamber to allow the measurements in forward direction. The intensities of the γ-rays at different angles were normalised to the monitor yields, corrected for the dead times and fitted to an expression

$$W(\theta) = A_0 + A_2 P_2(\cos\theta) + A_4 P_4(\cos\theta). \qquad /1/$$

The coefficients A_2 and A_4, after correction due to finite solid angles of the detectors used, are usually enough to determine the multipole nature /L=1,2,3/ of the γ-rays and hence the spins of the levels

The combination of the angular distribution data with the data from the electron conversion measurements suffices for an unambiguous assignment of the electric or the magnetic nature of the transitions. To determine conversion coefficients of the transitions, conversion electron spectra were measured with a mini-orange conversion electron spectrometer Different energy regions were selected using appropriate magnet configurations. To reduce the background of unwanted events only electrons in coincidence with a γ-ray registered by a multiplicity filter /consisting of four 7.6 x 7.6 cm NaJ/Tl/ detectors/ were recorded. The electron conversion coefficients were evaluated from the experimental electron intensities taking into account the efficiency of the electron spectrometer, the relative intensity of the γ-rays and the multiple nature of a few strong transitions.

The detailed information about the decay schemes of $^{163-167}$Yb obtained on the basis of the above mentioned studies and used in further discussion one can find in refs. [11,12,13,14,15].

3. The cranked shell-model

As it has already been mentioned in section 1, the nucleus is cold in the region of a few MeV excitation energy above the yrast line so its level density there is comparable with that near the ground state. The yrast spectra of deformed nuclei may be therefore understood in terms of configurations of quasiparticles in a potential rotating with a constant frequency about an axis perpendicular to the symmetry axis [10,21,23]. In recent years many yrast bands have been analysed on this basis [10]. This approach has also been very successful to interprete side bands and their band crossings [4,10,21]. In the present section some details concerning the cranked shell-model /CSM/ will be discussed.

The theoretical description is based on the single-particle routhian

$$h^{\omega} = h^{0} - \omega j_{1}, \qquad /2/$$

which is recognized as the hamiltonian in a reference frame rotating with angular frequency ω about the 1-axis, j_1 is the projection of the single-particle angular momentum on the axis of rotation /the 1-axis/. The hamiltonian h^0 is given by

$$h^{0} = h_{sp}/\xi/ + \Delta/P^{+} + P/ - \lambda N, \qquad /3/$$

where h_{sp} is the single-particle hamiltonian of the modified harmonic oscillator. A monopole pairing field P^+ with constant matrix elements is assumed. The strength of the monopole pairing field is fixed by the gap parameter Δ. The particle number N is determined by the chemical potential λ. The solution of the quasi-particle equations corresponding to h^{ω} is a set of quasi-particle energies e_i' as a function of the rotational frequency ω. The CSM considers the angular frequency as a physical quantity and extracts it from the experimental spectrum. It is next possible to transform the experimental energies into the rotating frame. These energies, called routhians, can be directly compared with

the spectrum of h^{ω}. In the CSM approach the same h^{ω} is assumed for all configurations. It implies that the energy and other quantities are equal to the sum of the contributions from the excited quasiparticles. The analysis of experimental data shows that an approximate additivity is observed. Deviations from the strict additivity are attributed to the residual interaction between the quasiparticles.

The presence of the second term in eq. /2/ violates the time-reversal and axial-symmetry. The routhian /2/ remains invariant with respect to both the space reflection and the rotation $R = R_1/\pi/$ of 180° about the axis of rotation /the 1 - axis/. The only good quantum numbers remaining for $\omega \neq 0$ are parity π /as a consequence of P-space inversion symmetry/ and the signature α. The quantum number arises from the invariance of h^{ω} with respect to the rotation $R_1/\pi/$, i.e.

$$R_1 h^{\omega} R_1^{-1} = h^{\omega}, \qquad /4/$$

with $R_1 = e^{-i\pi j_1}$ [10]. /5/

Therefore the single-quasiparticle states, $|\alpha_1\rangle$, of h^{ω} can be classified according to their symmetry with respect to R_1

$$R_1 |\alpha_1\rangle = e^{-i\pi\alpha}|\alpha_1\rangle. \qquad /6/$$

The quantum number α, defined in this way, is an additive quantity. For single-particle states, $\alpha = \pm 1/2$. For many-particle configuration the total α quantum-number is equal to the sum of the α quantum-numbers for all the occupied one-particle orbits. For example, two-quasiparticle configurations are characterized by the quantum-number $\alpha = 0, 1$.

As it has been mentioned above, the solution of the quasiparticle equations corresponding to h^{ω} is a set of quasiparticle energies e' as a function of the rotational frequency ω. It has to be

noticed, that the calculated quasiparticle energies are not absolute energies but relative to a reference spectrum, which in ref. 10 is defined as the energy spectrum of the ground band of an even-even nucleus. Results of a calculation for quasineutron configurations in ^{160}Yb [4] are shown in fig. 7, where for increased readability only positive parity levels are drawn. The quasiparticle orbits in fig. 7 are labelled with capital letters A,B,C ...

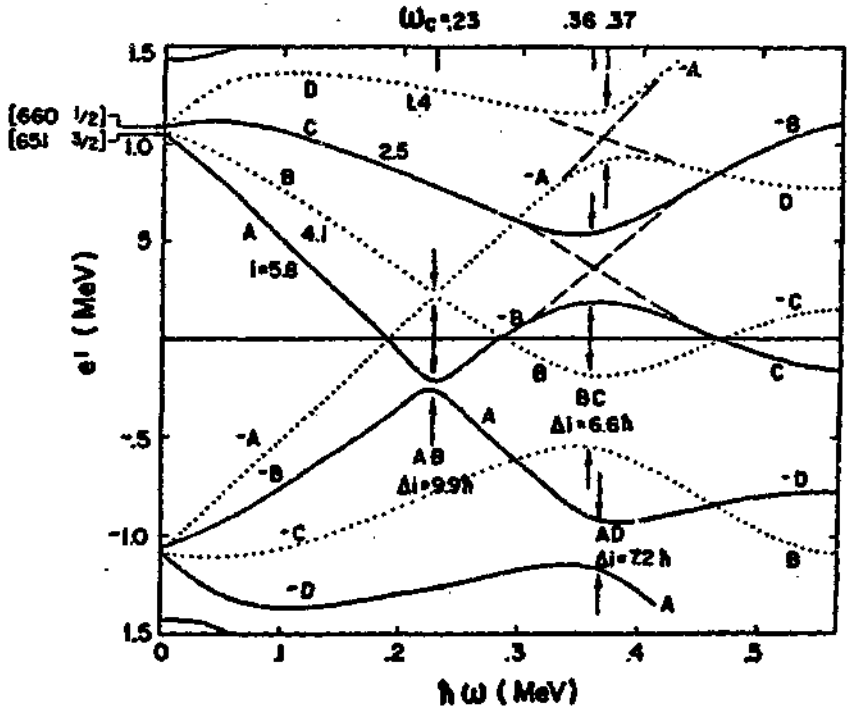

Fig. 7. Cranked shell-model calculation for N=90. Only positive parity levels are drawn. $\alpha = +1/2$ and $\alpha = -1/2$ are drawn in full and dotted lines, respectively. The slopes are th aligned angular momenta relative to the reference. The alignment gain, Δi, resulting from a crossing is equal to the sums of slopes of the interacting levels.

However, a more reasonable notation may be to write down a set of quantum-numbers $(\alpha,\pi)_n$, where n denotes that it is n^{th} configurations with the same quantum numbers. Some of the states in fig. 7 are labelled also with the asymptotic Nilsson quantum numbers, which are meaningful only at $\omega = 0$. The occupation of the quasiparticle states by quasiparticles is governed by the occupation number representation [10]. If, e.g., the level A (see fig. 7) is occupied, then the conjugate level -A, obtained by the reflection about $e' = 0$ and by change of the signature from α to $-\alpha$, must be free. Therefore, half of the levels are always occupied, and a quasiparticle excitation consists in occupying a level at $+e_i$ and freeing its conjugate partner, with resulting change of energy of the system. In an even-even nucleus the quasiparticle vacuum is obtained by filling all the negative energy states. For small frequencies this corresponds to the g-band (ground state band). The first excited two-quasiparticle band, corresponding to the S- band (i.e. the super or Stockholm band), is obtained by occupying the levels A and B. The S-band lowers in energy relative to the g-bands as a result of the rotation. The quasiparticle states A and B would cross -B and -A at $\hbar\omega \approx 0.27$ MeV if there were no repulsion and exchange of characters. After the crossing, the S-band is the vacuum state and the g-band is the first excited state. The band crossing causes the irregularity in the yrast band, hitherto called backbending. Crossings between other quasiparticle trajectories may also occur and are identified in fig. 7 by the repulsion between trajectories corresponding to the same values of α and π.

In the section 8 the CSM calculations will be discussed in more details and compared with observed rotational bands in Yb nuclei.

4. Transformation of the decay-scheme information to e′ versus ħω representation

To study the effect of rotation on an independent-particle motion in a deformed nucleus, it is convenient to transform the decay-scheme information i.e. lab-frame excitation energies, E_x, and angular momentum, I, into excitation energies in the rotating intrinsic frame (routhians, e′) and angular frequency ω ($\hbar\omega = \frac{E_\gamma}{2}$ for $\Delta I = 2$). In the e′ versus ħω representation, the ħω dependence of the intrinsic excitation energy of the nucleus can be studied for the specific nuclear configurations which are basic for the rotational sequences in the decay schemes.

In order to calculate the experimental routhian, the rotational frequency has to be determined. The rotational frequency with which the potential rotates about the x-axis can be obtained by approximating the classical relation

$$\omega = \frac{d\,E(I)}{d\,I_x}\,, \qquad /7/$$

by the quotiant of finite differences

$$\omega(I) = \frac{E(I+1) - E(I-1)}{I_x(I+1) - I_x(I-1)}\,, \qquad /8/$$

where $E(I+1)$ and $E(I-1)$ are two consecutive states of the same signature in a rotational band and I_x is the angular momentum component on the rotational axis in units of ħ. Semiclassically, the component I_x is determined as

$$I_x(I) = \sqrt{(I + 1/2)^2 - K^2}\,, \qquad /9/$$

where K is the angular momentum component along the symmetry axis. The energy in the rotating frame is then given by

$$E'(I) = \frac{1}{2}\left[E(I+1) + E(I-1) - \omega(I)\, I_x(I)\right]. \qquad /10/$$

In the case of odd mass nuclei the energy must be counted from the ground state of an even-even neighbour, i.e. the even-odd mass difference, Δ_{eo}, must be added to the experimental excitation energies.

As pointed out earlier to compare E' and I_x for different nuclei and with CSM calculations, it is necessary to establish a reference frame and to consider the relative routhians, e', and aligned angular momenta, i,

$$e'(\omega) = E'(\omega) - E_r(\omega). \qquad /11/$$

$$i(\omega) = I_x(\omega) - I_{xr}(\omega). \qquad /12/$$

Two choices of reference frames are in common use for even-even nuclei: the ground state configuration [10] and the yrast configuration [18]. There are technical problems associated with both choices of the reference frames which are discussed below. The ground-state band moment of inertia is not constant at the lowest $\hbar\omega$ and this band is not known at higher $\hbar\omega$. Therefore, for the reference it is necessary to choose an appropriate parameterized reference as a function of $\hbar\omega$ to approximate the zero-quasiparticle ground state configuration. The reference frame chosen in this paper is a band with a variable moment of inertia [19] described by the Harris formula [20]

$$J = J_0 + \omega^2 J_1 . \qquad /13/$$

The Harris parameters used in establishing the "ground-state" reference are collected in table 1. These parameters, which are similar to those used for lighter Yb isotopes [21,22], are the compromise between the values necessary to produce constant alignment in the ground-state band (J_1 125 MeV$^{-3}\hbar^4$ in ^{166}Yb) and in the yrast sequence above the lowest-frequency band crossing,

the S-band [23], (J_1 70 MeV$^{-3}\hbar^4$). The choice of average parameters, which vary smoothly from nucleus to nucleus (J_1 constant and J_0 only slightly N dependent), makes it possible to discuss the systematics of the rotational effects for quasiparticle state in neighbouring isotopes and isotones. However, the use of such a average reference frame results in a slight increase in the alignment with increasing frequency in the ground-state band and a small decrease in i with $\hbar\omega$ in the S-band.

TABLE 1. Harris parameters used for the ground-state reference

Nucleus	J_0 MeV$^{-1}\hbar^2$	J_1 MeV$^{-3}\hbar^4$
^{163}Yb	23	90
^{164}Yb	25.8	90
^{165}Yb	27.8	90
^{166}Yb	29.8	90
^{167}Yb	31.8	90

For odd-N or odd-Z nuclei the routhians and aligned angular momenta are referred to the appropriate reference configuration of the neighbouring even-even nuclei and the quasiparticle energy E_ν, of the ground-state configuration for the odd-A nucleus

$$E_\nu = \sqrt{\Delta^2 + (\varepsilon_\nu - \lambda)^2}, \qquad /14/$$

is added. In the deformed region the spacing of the Nilsson level is usually such that the energy of the ground-state relative to the Fermi surface, $\varepsilon_\nu - \lambda$, can be ignored and $E_\nu \approx \Delta$.

Problems associated with the extrapolation of the ground-state

reference frame to higher $\hbar\omega$ can be avoided by referring the intrinsic-frame excitation energies to the yrast band. The yrast configuration of even-even nuclei, however, is not necessarily appropriate for the neighbouring odd-mass isotopes and isotones. For example, a difference in pairing and interaction strengths between odd- and even-N or Z neighbours will produce changes in the references appropriate for odd- and even-N or Z nuclei. Such problems will be discussed farther on (see section 8) where experimentally constructed routhians are compared directly with CSM calculations. Information about alignment, i, is also contained in the e'' vs $\hbar\omega$ plots as

$$i = \sum j_1 = - \frac{de'}{d\omega} \quad . \qquad /15/$$

It is often convenient to plot i vs $\hbar\omega$ because of the similarity of such a presentation of the data with the familiar "backbending" plot.

Routhians and alignments are shown in fig. 8 as a function of $\hbar\omega$ for the yrast sequence of ^{166}Yb referred to both the ground-state band and the yrast references. Near $\hbar\omega$ for which the "backbending" effect occurs the excitation energy of the yrast sequence is double-valued for a particular $\hbar\omega$.
It is, therefore necessary to define which branch of the yrast sequence should be taken as the reference frame: for $\hbar\omega < \hbar\omega_c$ the ground-state band is used while for $\hbar\omega > \hbar\omega_c$ the S-band is taken as the reference. The appearance of a crossing of the weakly-interacting bands in e' and i plots referred both to the ground-state and to the yrast configurations can be seen in fig. 8.

Since the present paper is confined to relatively low values of $\hbar\omega$, where the extrapolation of the ground-state configuration is reasonable, the data will usually be referred to a parameterized ground-state configuration eq. 13 . For example, the information on e' vs $\hbar\omega$ gained from the experimental levels schemes of ^{161,163,165}Yb is shown in fig. 9, after the transformation to the

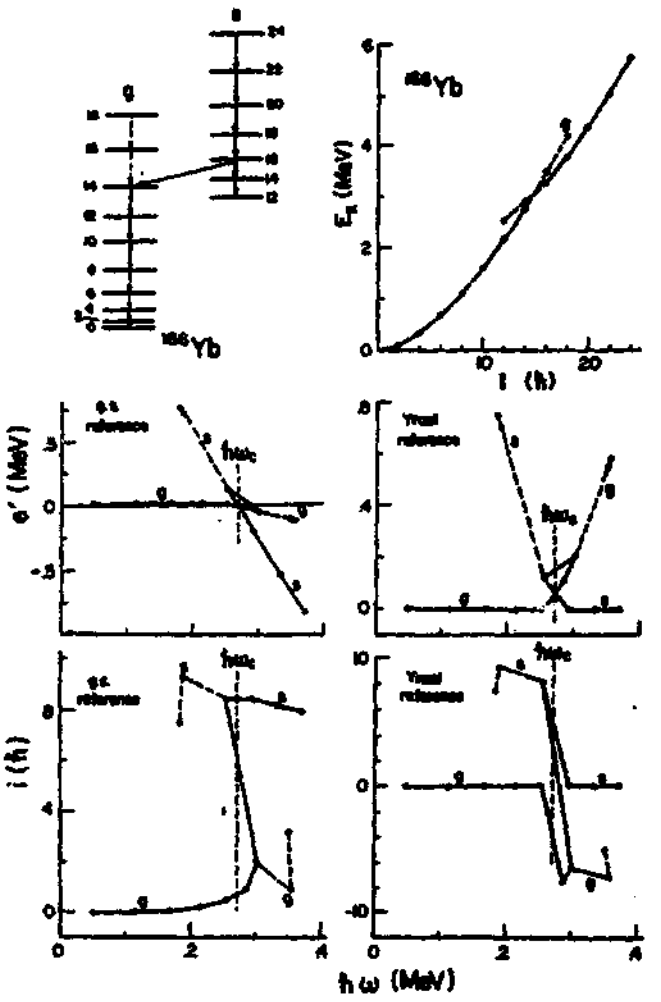

Fig. 8 Routhians, e', and alignments, i, as a function of $\hbar\omega$ for the ground-state band and the S-band in ^{166}Yb referred to the g.s.b. reference (shown to the left), and to the yrast reference (shown to the right). A partial decay scheme of ^{166}Yb and an E_x versus I plot showing the levels of the g.s.b. and the S-band are also shown in the upper portion of the figure.

rotating frame and it is referred to the ground-state configuration. In ^{167}Yb, however, where there are strong interactions between the quasiparticle configurations, it is more convenient to choose an yrast reference.

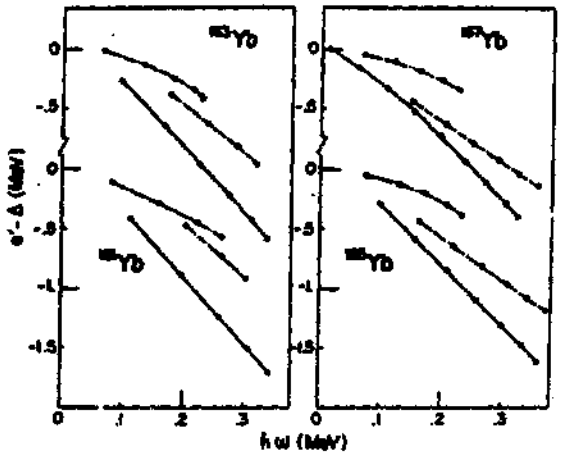

Fig. 9. Experimental routhians for bands assigned to the $(+,+)_1$, $(+,-)_1$ and $(-,+)_1$ configurations (designated by solid, dashed and dot-dashed lines, respectively) in ^{161,163,165,167}Yb, referred to the ground-state bands and their smooth extrapolations.

5. The spectrum of single-quasineutron states in odd-A Yb isotopes

Before comparing experimental routhians with calculated excitation energies for independent-particle motion in a rotating, deformed potential, the spectrum of the experimental single-quasiparticle states which can be obtained from odd-A nuclei will be discussed. The rotational configurations are labelled by the conserved quantum numbers of the corresponding intrinsic quasiparticle configurations $(\pi,\alpha)^S_n$, parity, π, and signature, α, (+ or - corresponds to $\alpha = 1/2$ or $-1/2$, while for $\alpha = 0$ or 1 it is explicitly stated). A superscript S is added to multi-quasiparticle states to assign the seniority of the configuration The π of a multiple-quasiparticle configuration is the product of all the constituent quasiparticles, whereas the α of the multiple-quasiparticle configuration is the sum of the α's of the constituent quasipartioles.

In the odd-A Yb isotopes (see e.q. the level scheme of ^{165}Yb shown in fig. 3) three bands are known which are interpreted [12,14,24] as single-quasineutron intrinsic configurations: the ground-state band with $(\pi,\alpha)_n = (-,+)_1$, and the favoured and unfavoured portions of the yrast band with $(\pi,\alpha)_n = (+,+)_1$ and $(+,-)_1$, respectively. The systematics of the single-quasiparticle routhians are such as expected from the Nilsson states near the Fermi surface (see fig. 10). The $K = 3/2^-$ ground state bands in ^{161}Yb and ^{163}Yb and the $K = 5/2^-$ ground-state bands in ^{165}Yb and ^{167}Yb are based dominantly on the $h_{9/2}$ and $f_{7/2}$ shell-model states. Therefore, because of the relatively large Ω in comparison with j, these configurations are expected to achieve only a small alignment during rotation. In contrast, the yrast bands are expected and observed to have larger rotational alignments. These bands are based on the $(+,+)_1$ and $(+,-)_1$ intrinsic configurations that at $\hbar\omega = 0$ correspond to the $5/2^+[642]$ Nilsson configuration. Furthermore, $3/2^+[651]$ and $1/2^+[660]$ Nilsson configurations which may have very large rotational alignment are sufficiently close to the Fermi surface (see fig 10) to mix into

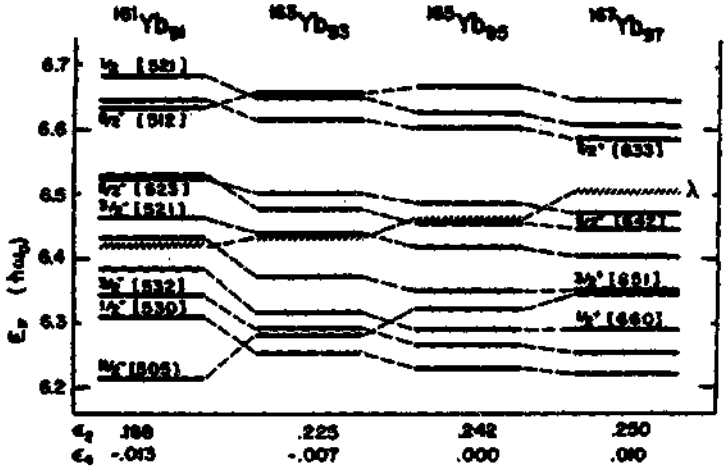

Fig. 10. Position of the Fermi surface, λ, relative to the Nilsson levels for ^{161,163,165,167}Yb. The spectrum of the Nilsson levels was calculated with the quadrupole and hexadecapole deformations suggested by Bengtsson [46] and given in the figure. The position of the Fermi surface was determined by requiring that the nucleus has the correct neutron number.

the yrast configuration at higher $\hbar\omega$.

Under rotation K is no longer a constant of the motion, therefore, the $\Omega = K = 1/2$ component is mixed into the other configuration producing a "signature-dependent splitting" between the $\Omega = \pm 1/2$ components of all the configurations. The energy splitting between the routhians corresponding to the different signatures of the yrast configuration, i.e. $(+,+)_1$ and $(+,-)_1$, is a measure of the $\Omega = 1/2$ component in the wave function. The systematic decrease with increasing N in both, the alignment of the yrast bands and the energy splitting [12,14,24] between the different signatures of the yrast bands (see fig. 11) is a consequence of the movement of the Fermi surface toward $i_{13/2}$ orbits of large Ω (see fig. 10).

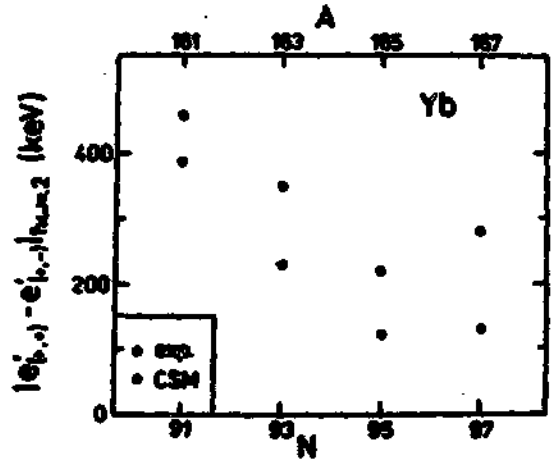

Fig. 11. Experimental and calculated (CSM) signature splitting of the yrast bands in odd-A Yb nuclei at $\hbar\omega$ = 0.2 MeV.

6. Construction of multiple-quasineutron states from the spectrum of single-quasineutron states

The single quasineutron states such as the three observed experimentally, in the odd-A Yb isotopes, represent the "building blocks" for the construction of multiple-quasineutron states. From the energies of these single-quasineutron states in the intrinsic system it is possible to construct the excitation energies as a function of $\hbar\omega$ for multiple-quasiparticle states. For example, the routhians corresponding to the two lowest expected two-quasiparticle, negative-parity configurations $(-,0)^2_1$, and $(-,1)^2_1$ and the lowest two-quasiparticle, positive-parity configurations, $(+,0)^2_1$, in the neighbouring even-mass Yb isotopes as well as the lowest three-quasineutron configuration, $(-,+)^3_1$ of the odd-mass Yb isotopes can be constructed as simple sums of the routhians of the single-quasineutron configurations $(+,+)_1$, $(+,-)_1$ and $(-,+)_1$ of the odd-mass Yb's. The construction of two- and three quasineutron routhians from combinations of three single-quasineutron routhians observed in odd-Yb isotopes is shown schematically in fig. 12. In this figure no value for the neutron pairing-correlation parameter, Δ_n, has been assumed. Instead Δ_n are obtained when the constructed routhians are compared with experimental two- and three-quasineutron routhians. Two of the constructed two-quasineutron configurations, $(+,0)^2_1 = [(+,+)_1 \otimes (+,-)_1]^2_1$, i.e. the S band, and $(-,1)^2_1 = [(+,+)_1 \otimes (-,+)_1]^2_1$ the lowest negative - parity band, are known in the even-A Yb's. Similarly, the three-quasineutron configuration, $(-,+)^3_1 = [(+,+)_1 \otimes (+,-)_1 \otimes (-,+)_1]^3_1$ is known as the ground-state band in the odd-A Yb's above the observed band crossing. From the comparison between the routhian of multiple-quasiparticle states and routhians constructed from experimental single-quasiparticle states, it can be found out where the strong $\hbar\omega$-dependent and configuration-dependent residual interactions between the constituent quasiparticles in the multiple-quasiparticle configurations exist. In the cranked shell-model [10] it is assumed that such

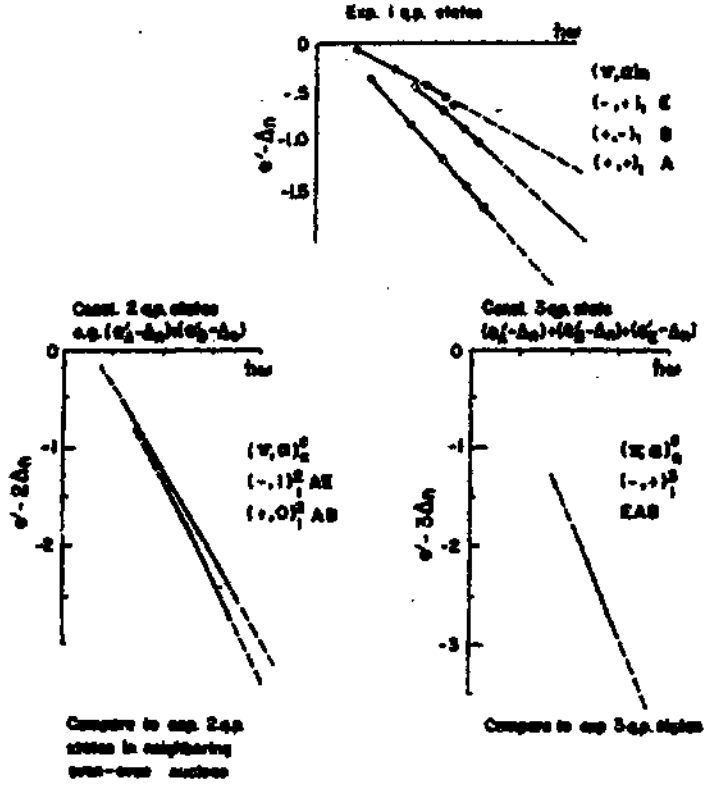

Fig. 12. Schematic figure illustrating construction of 2- and 3- q.p. routhians using 1-q.p. routhians. Note that the neutron pairing correlation parameter, Δ_n, has not been added to the routhians. The dashed lines represent routhians for those ranges of $\hbar\omega$, for which routhians for one or more constituent quasiparticles have been extrapolated.

residual interactions between quasiparticles are weak. Thus, from the comparison discussed above one can decide whether the CSM can be applied.

It is also possible, as has been already mentioned, to obtain information on the neutron pairing-correlation parameter, Δ_n, from the comparison of the absolute excitation energies of the constructed and experimental multiple-quasineutron routhians. Since the single-quasiparticle levels usually are referred to the ground-state configuration of the neighbouring even-even nuclei, it is necessary to include, as a constant factor, the quasiparticle energy, $E_{\nu} \simeq \Delta$, in the odd-A routhians. Instead of including, for example, the odd-even mass difference as an estimate of Δ_n into the odd-A routhians, it is chosen to keep Δ_n as a parameter and to plot $e' - \Delta_n$ for the odd-A systems. Then the energy difference between the constructed two-quasineutron systems, $e'_{2qp} - 2\Delta_n$, and the experimental values in the neighbouring even-even systems, e'_{2qp}, will give a measure of Δ_n. The values of Δ_n obtained from such a comparison will be labelled Δ_n^{ce} to emphasise that they were obtained as a diffsrence between two-quasineutron routhians, constructed as a sum of "experimental" single-quasineutron routhians and "experimental" two-quasineutron routhians. From a similar comparison of the constructed and the experimental three--quasineutron states a measure of Δ_n^{ce} can be also obtained, since Δ_n appears in the constructed three-quasineutron state three times (once in the $e' - \Delta_n$ for each quasineutron) and only once in the construction of the experimental routhian for the three--quasineutron state.

Two quasineutron routhians constructed for the $(+,0)^2_1$ and $(-,1)^2_1$ states are compared to the experimental ones for ^{160,162,164,166}Yb in fig. 13. In the construction of the two-quasineutron routhians average values of the appropriate single-quasineutron routhians in the neighbouring odd-A isotopes were used. Such an averaging ought to remove at the first approximation, effects which vary smoothly with neutron number. In fig. 13 the constructed two-quasineutron routhians i.e. $e_{2qp} - 2\Delta_n$ were shifted up by two times the Δ_n value given in the figure in order to reproduce the experimental values. Both the slope (i.e. the alignment) and the energy splitting of the experimental routhians for

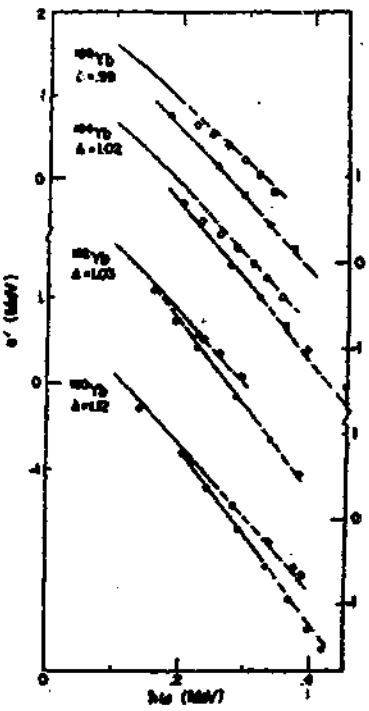

Fig. 13. Comparison of the experimental (circles) and the constructed - see fig. 12 - (solid and dashed lines) routhians for 2-q.p. bands in ^{160,162,164,166}Yb. The open and the closed circles represent the experimental routhians for the odd-spin, odd-parity bands and the s-bands, respectively. The dashed lines represent the constructed routhians for those ranges of $\hbar\omega$, for which routhians for one or more constituent quasineutrons have been obtained by extrapolation. The energy scales on the left-hand and right-hand sides correspond to ^{162,166}Yb and ^{160,164}Yb, respectively. The experimental data for ^{160}Yb and ^{162}Yb were taken from refs. 21,24. For further details, see text.

the lowest positive- and negative-parity two-quasineutron configurations are reproduced by routhians constructed as the sum of the routhians of single-quasineutron configurations. Such an agreement indicates that a residual interaction between the two unpaired quasiparticles is not strongly dependent on the angular frequency and the quasiparticle configurations.

The constructed three-quasineutron routhians for the $(-,+)^3_1$ configuration $\left(= e'(+,+)_1 + e''(+,-)_1 + e'(-,+)_1 \right)$ are also compared in fig. 14 with the routhians of the ground-state bands of ^{161,163,165,167}Yb's above the band crossing. A smaller alignment is observed in the three-quasineutron configurations of these nuclei than it is expected from the experimentally construced routhians. A possible explanation is the following: when three-quasineutron

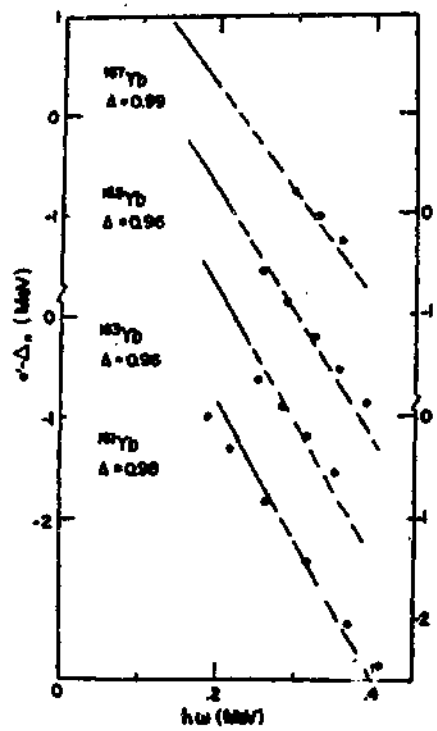

Fig. 14. Comparison of the experimental (circles) and the construcoted - see fig. 12 - (solid and dashed lines) routhians for the lowest negative-parity 3 q.p. bands, $(-,+)_1 \otimes [(+,+)_1 \otimes (+,-)_1 \otimes (-,+)_1]_1$ in ^{161,163,165,167}Yb. The dashed lines represent the constructed routhians for those ranges of $\hbar\omega$, for which routhians for one or more constituent quasineutrons have been obtained by extrapolation. The energy scales shown to the left-hand and the right hand sides correspond to ^{163,167}Yb and ^{161,165}Yb, respectively. The experimental data for ^{161}Yb were taken from ref. 24. For further details, see text.

orbits near the Fermi surface are occupied, thereby "blocking" their contribution to pairing, the pairing is sufficiently reduced to decrease the alignment. Cranked shell-model calculations do indicate that a decrease in the alignment is associated with the decreased pairing. Therefore, the present agreement in the alignments for the construoted and experimental two-quasinoutron states together with the deviation for the three-quasineutron states would indicate a significant decrease in Δ_n for the three-quasineutron configurations when compared to the two-quasineutron configurations. Since there is a discrepancy between the slopes of the constructed and the experimental three-quasineutron routhians, it is not possible to get an estimate of Δ_n from the energy difference between these routhians.

The described above method of constructing multiple-quasiparticle routhians on the basis of single-quasiparticle ones as "building blocks" and comparing with the experimental routhians can be extended to more than three quasiparticles [22].

7. Band-crossing systematics in Yb nuclei

In the mass region, where the Fermi surface is near the low-Ω $i_{13/2}$ neutron orbits, the band-crossing frequency, $\hbar\omega_c$, corresponding to the alignment of the first pair of neutrons, is controlled by a rotational aligned orbit near the Fermi surface which is particularly sensitive to the neutron pairing-correlation parameter [25].

To establish the angular frequency, $\hbar\omega_c$, at which it is energetically favourable for a quasineutron pair to be aligned, it is convenient, as it has been mentioned before, to express the information contained in the level schemes in a rotating frame. Nonrotational features, interpreted as the band crossings, are apparent from the variation of $\mathcal{J}^{(2)}$ as a function of $\hbar\omega$ for a specific cascade (see fig. 8). The band-crossing frequencies, $\hbar\omega_c$, are well determined from such a plot. In even-even rare-earth nuclei the lowest-frequency band crossing corresponds to the crossing of the ground-state band with the aligned two-quasineutron S-band. This band-crossing which corresponds to the alignment of a pair of $i_{13/2}$ quasineutrons, is responsible for the backbendings observed in the yrast sequence of even-even rare-earth nuclei. A band crossing corresponding to the alignment of the same two quasineutrons can also be observed in the low-lying negative-parity bands of the odd-N nuclei. Here a band based on the negative-parity single quasineutron crosses a three quasineutron band involving the unpaired negative-parity quasineutron as well as the same two $i_{13/2}$ quasineutrons which form the configuration of the S-band in the even-even nuclei.

Experimental band-crossing frequencies for a large number of Yb nuclei [11,12,13,14,24,26,27], Er [28-33], Hf [34-38] and W [39,40] nuclei are shown as a function of the neutron number in fig. 15. In the mass region presented in this figure, the $\hbar\omega_c$ for odd-N nuclei is systematically, 40-50 keV, lower than for even-even nuclei. As will be shown below, this systematic lowering of $\hbar\omega_c$ when going from odd- to even-N nuclei is not a result of the technique of defining $\hbar\omega_c$ from the experimental routhians.

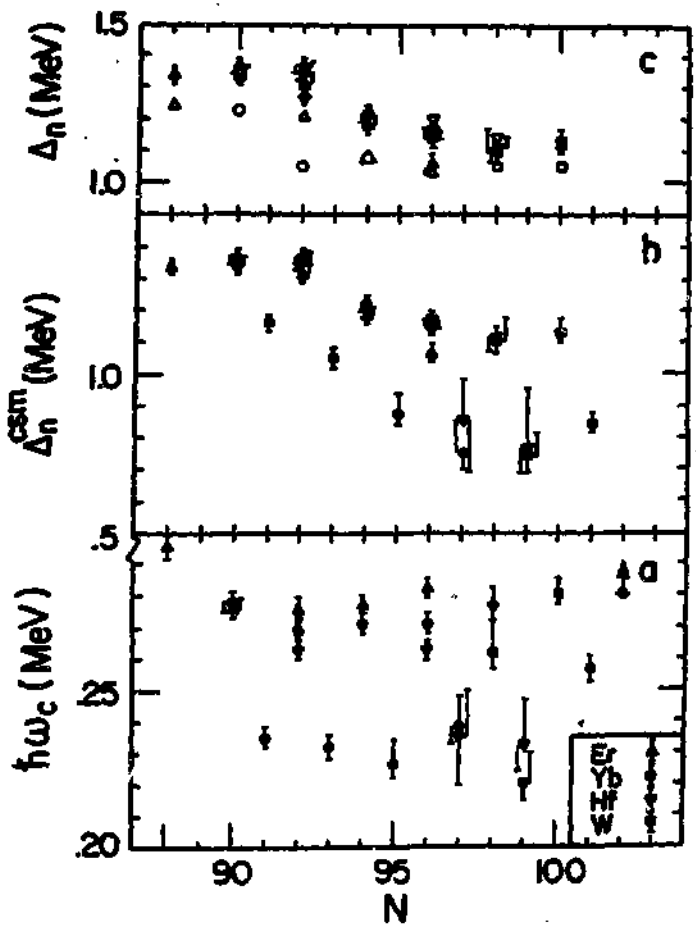

Fig. 15. a/ Systematics of $\hbar\omega_o$ for yrast bands in even-mass nuclei and for the lowest negative-parity band in odd-N nuclei.
b/ Values of Δ_n^{CSM} necessary to reproduce the value of $\hbar\omega_c$'s in CSM calculations. The error bars only reflect uncertainties in the definition of the $\hbar\omega_c$'s and do not include model-dependent uncertainties resulting from the CSM calculations.
c/ A comparison of Δ_n^{CSM} for even-N systems (solid symbols) with Δ_n^{oe} (open symbols) obtained from odd-even mass differences.

The crossing frequencies are nearly independent of the Harris parameters used to remove the excitation energy of the rotating core. If a nonzero value of K is assumed for the S-band, the magnitude of the odd-even variation of $\hbar\omega_c$ would be even larger.

In order to determine whether the observed shift in $\hbar\omega_c$ is a function of neutron number or mass number, the nuclei ^{157}Hf and ^{159}Tm were studied [41,42]. The observed $\hbar\omega_c$ for odd-Z, even-N nuclei are characteristic of the even-even nuclei, therefore, the variation in band-crossing frequencies is dependent on whether there is an even or odd number of neutrons. Such a shift of $\hbar\omega_c$ or neutron alignment frequencies to lower angular frequencies for odd-N systems can be explained by a reduction of the neutron pairing-correlation parameter, Δ_n, for the odd-N nuclei (see fig. 16). If there is less pairing, the rotational aligned configuration becomes yrast at a lower $\hbar\omega_c$.

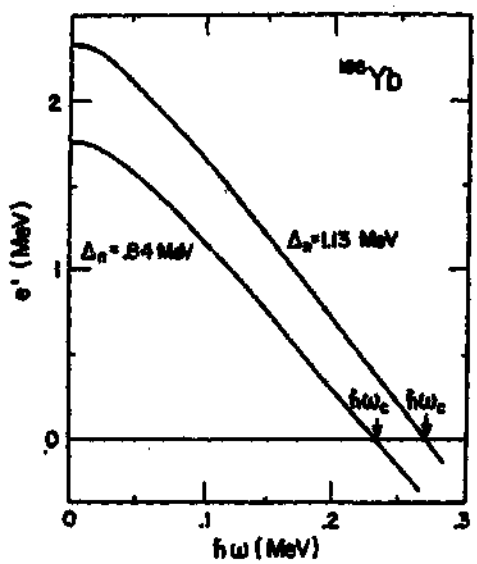

Fig. 16. Cranked shell-model two-quasineutron routhians calculated as a function of $\hbar\omega$ for ^{166}Yb with ϵ_2= .246 and ϵ_4= .005 and two different values of Δ_n (0.84 and 1.13 MeV). The shift in $\hbar\omega_c$ corresponding to a change in Δ_n is indicated.

Qualitative evidence for a reduction of Δ_n in odd-N nuclei as compared to the seniority-zero bands in the even-even nuclei was obtained previously from the analysis of the moments of inertia, α-decay intensities and two-nucleon transfer cross sections [8]. From these techniques, however, due to uncertainties associated with the calculations of the moments of inertia, α-decay and particle-transfer cross sections it is difficult to get accurate quantitative values for the magnitude of the pairing reduction. The fact that the reduction in the pairing energy is measured as an energy (i.e. the shift of the crossing frequency) suggests that the procedure to get quantitative values of the pairing reduction may be less complicated than that for the other techniques. It is only necessary to predict correctly the average alignment for frequencies $0 \leqslant \hbar\omega \leqslant \hbar\omega_c$ (see fig. 16) to obtain a measure of the change in Δ_n, i.e. $\delta\Delta_n$, associated with the shift in $\hbar\omega_c$.

In the small region around the critical frequency $\hbar\omega_c$ where the trajectories of the positive and negative-energy quasiparticles approache each other the CSM [43] does not describe well the motion of the quasiparticles. The cranked shell-model reproduces experimental alignments over the remaining range of $\hbar\omega_1$. Thus, it is expected that the absolute values of Δ_n labelled Δ_n^{CSM} obtained from the CSM analysis of the crossing frequencies, given in fig. 15b, are a reasonable measure of the neutron pairing-gap parameter for the nuclei $\hbar\omega_c$ of which is controlled by high-j low-Ω orbits near to the Fermi surface. Indeed, as it is shown in fig. 15c, the values of Δ_n^{CSM}, extracted for even-even nuclei are in agreement with odd-even neutron mass differences, Δ_n^{oe}, for those systems where accurate mass measurements exist [44].

A reduction in the alignment of the lowest frequency pair of $i_{13/2}$ neutron should be also associated with the reduction of Δ_n in the odd-N system. A systematics of such a reduction in odd-N Yb nuclei for the $i_{13/2}$ neutron alignment with respect to the alignment of the same pair of $i_{13/2}$ neutrons in even-even nuclei as well as with respect to the sum of the alignments of the single-quasineutron states corresponding to the two active $i_{13/2}$ quasineutrons is presented in fig. 17.

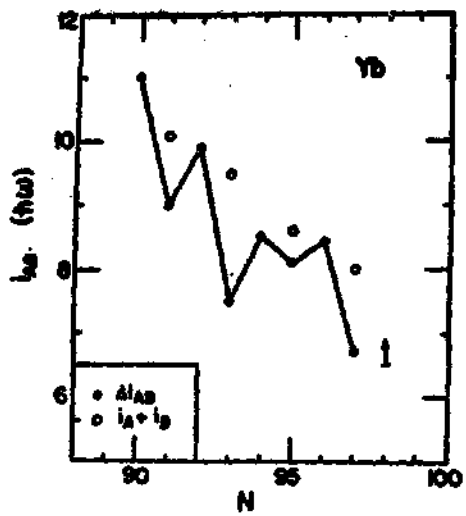

Fig. 17. Systematics of the alignment in Yb nuclei for the first pair of $i_{13/2}$ neutrons (i.e. $(+,+)_1 \equiv$ A and $(+,-)_1 \equiv$ B) taken from the gain in the alignment at the lowest-frequency band crossing (closed circles) and from the sum of alignments of the corresponding single-quasineutron states in odd-N nuclei (open circles).

8. Comparison with cranked shell-model calculations

The best test of the cranked shell-model is a direct comparison of calculated routhians with "experimental" ones obtained from the decay scheme information. The parameters used in the CSM - calculations are the quadrupole deformation ε_2, the hexadecapole deformation ε_4, the pairing-correlation parameters Δ_n and Δ_p (for neutrons and protons, respectively) and the chemical potential λ which determines the expectation value of the particle number. In the rare-earth region the quadrupole and hexadecapole deformations, ε_2 and ε_4 are rather well known and were taken from the systematics published by the Lund-Warsaw group [45,46]. As discussed earlier, one can obtain an estimate of Δ_n from the $\hbar\omega_c$ crossings frequencies of the ground-state bands in odd-N Yb nuclei. (The parity, π = -, of the ground-state band assures that none of the $i_{13/2}$ neutron configurations, π = +, is "blocked". The procedure then is to take this Δ_n value together with deformation parameters, ε_2, ε_4 and the appropriate position of the Fermi surface, λ, to reproduce the neutron number, and to calculate the spectrum of the single-particle states in the rotating intrinsic frame. The results of such CSM-calculations for ^{165}, ^{167}Yb's are shown in fig 18.

It is possible to compare directly these predicted quasiparticle levels with the experimental routhians constructed (see section 3) from the decay scheme information. However, with the ground-state configuration taken as the "reference" for all angular frequencies, it appears necessary to reconstruct the pure quasineutron states in these regions where the mixing between the quasiparticle states is substantial [10,47]. When the interactions are strong and/or several levels interact, such a reconstruction, becomes impossible. The technique described in refs. 10 and 47 is used in the present work to obtain the pure quasineutron states in the interaction regions for ^{161,163,165}Yb. The resulting theoretical and "experimental" routhians are presented in fig. 19. In the calculation of the experimental

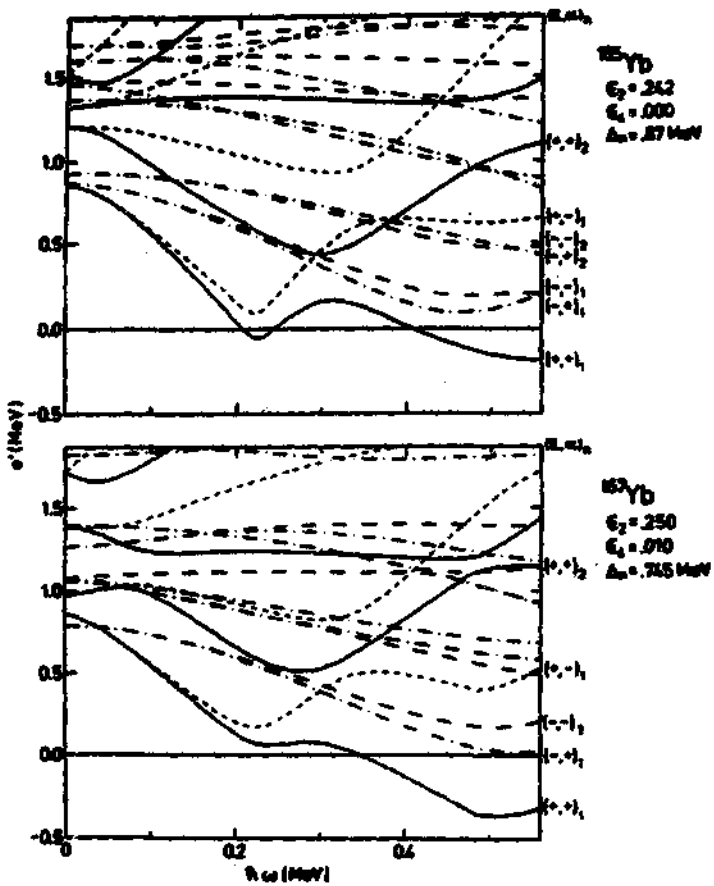

Fig. 18. Quasineutron levels in the rotating frame for $^{165,167}Yb$, obtained from CSM calculations and shown as a function of the rotational frequency $\hbar\omega$. The parameters used, and the parities and signatures of a few trajectories are shown to the right. $(\pi,\alpha) = (+,+)$, $(+,-)$, $(-,+)$ and $(-,-)$ states are indicated by full drawn, short-dashed, and long-dashed lines, respectively.

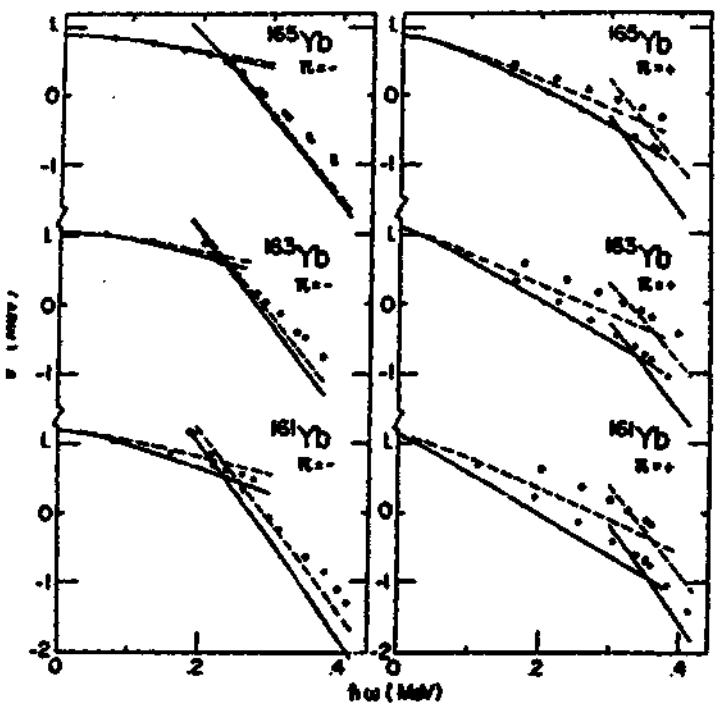

Fig. 19. Comparison of the experimental quasineutron spectra for ^{161,163,165}Yb, shown as a function of $\hbar\omega$, with those from CSM calculations. The filled circles and the solid lines are the experimental and the theoretical spectra, respectively, for bands with positive signature. The open circles and the dashed lines depict the same for bands with negative signature. The experimental data for ^{161}Yb were taken from ref. 24.

routhians, the values, Δ_n, necessary to reproduce the band crossing in the ground-state band [25] have been assumed. At angular frequencies below the band-crossing frequencies, where the routhians correspond to single-quasineutron configurations,

the alignment and the relative excitation energies of the lowest positive- and negative-parity configurations in ^{163,165}Yb, $(+,+)_1$ and $(-,+)_1$ are reproduced well. For ^{161}Yb, however, the positive-parity configuration is predicted to be the closest to the Fermi surface even for small $\hbar\omega$, in disagreement with the experimentally observed negative-parity ground state [24]. The observed energy splitting between the two signatures of the positive-parity configurations, $(+,+)_1$ and $(+,-)_1$, is greater than predicted. A similar discrepancy has been observed for several other rare-earth nuclei [10]. For $\hbar\omega<h\omega_1$ a larger than observed alignment is predicted for both negative-parity three-quasineutron configurations, $(-,+)^3_1$ and $(-,-)^3_1$. The observed alignment for these configurations is also less than that of the three-quasineutron routhians constructed as a sum of the appropriate single-quasineutron routhians (see section 6). The alignment of the three-quasineutron configurations can be reproduced in the CSM-calculations if the pairing-correlation parameter is reduced by 25% relative to the value of Δ_n^{CSM} obtained from one- and three-quasineutron band crossing frequencies.

Band crossings are also predicted in the positive parity bands (see fig. 19), $(+,+)_1$, corresponding to the alignment of a different pair of $i_{13/2}$ quasineutrons than those responsible for the lower frequency alignment in the negative-parity band and in the yrast band of the neighbouring even-N isotopes. This band-crossing frequency is correctly reproduced in ^{161}Yb and ^{163}Yb but it is observed at about 50 keV higher in $\hbar\omega$ than predicted in ^{165}Yb. Of course, it is possible to increase the frequency of this band crossing in CSM-calculations by an arbitrary increase in the pairing correlation parameter. However, to reproduce the observed crossing frequency, it is necessary to increase Δ_n by about 35% with respect to the value used to reproduce the lower-frequency crossing in the negative-parity band. Such an increased value of Δ_n is as large as that derivod from the ground-state band- S-band crossing in the neighbouring even-N Yb isotopes [25]. It is, however, difficult to understand in a phenomenological way how the occupancy of certain single-particle configurations in some

odd-N Yb nuclei significantly reduces Δ_n while in others does not affect it. As a matter of fact, the recent calculations done by R. Bengtsson and J-y. Zhang [48] suggest that for neutron levels in rare-earth nuclei, the pairing is reduced more for the negative-parity states than for the positive-parity states and for configurations with smaller signature splitting. Such effects might play a role in explaining the observed discrepancy in the band crossing frequency in the positive-parity band in ^{165}Yb. However, the observed signature splittings between positive--parity states in ^{161}Yb and ^{163}Yb are larger than in ^{165}Yb, therefore, such an effect would seem to be the largest in the lighter odd-N Yb isotopes where the band crossing is predicted at the correct frequency. In the case of ^{165}Yb, it is also difficult to alter significantly the difference in $\hbar\omega$ between the predicted crossings for the negative-parity and positive-parity bands by small changes in the various parameters which are taken into account in the CSM-calculations. Thus the source of the discrepancy in ^{165}Yb is not understood yet.

The frequency of the crossing in the favoured and unfavoured positive-parity band (which corresponds to the exchange of the roles of the $(+,\pm)_1$ and $(+,\pm)_2$ trajectories - see fig. 18) represents a more thorough test of the CSM than the lowest-frequency band crossing (i.e. that observed in the negative parity band). The $(+,\pm)_1$ - $(+,\pm)_2$ crossings are sensitive to the quasiparticle energy, alignment and the interaction of the trajectories. The $(+,\pm)_2$ and the higher laying trajectories are derived from and interact with Nilsson orbitals which are more distant from the Fermi surface (see fig. 10). Therefore, not only the relative positions of orbits, but also their energy relative to the Fermi surface, $\varepsilon - \lambda$, becomes important in predicting the higher-frequency band crossings. Furthermore, the strengths of the interactions at the lower-frequency crossings are also important in the calculation of the higher-frequency crossings.

When the interaction between the quasiparticle trajectories is strong, it becomes difficult to reconstruct the "pure" quasiparticle trajectories in the interaction region. In the case of

^{167}Yb (see fig. 18), where there are two strongly interacting trajectory crossings closely spaced in angular frequency corresponding to the alignment of the first and the second pair of $i_{13/2}$ neutrons , it is particularly difficult to reconstruct the "pure" quasiparticle trajectories. Such troubles can be avoided by referring the experimental routhians to the yrast band in the neighbouring even-even isotopes. Then, the experimental routhians can be directly compared to the calculated routhians (see fig 20).

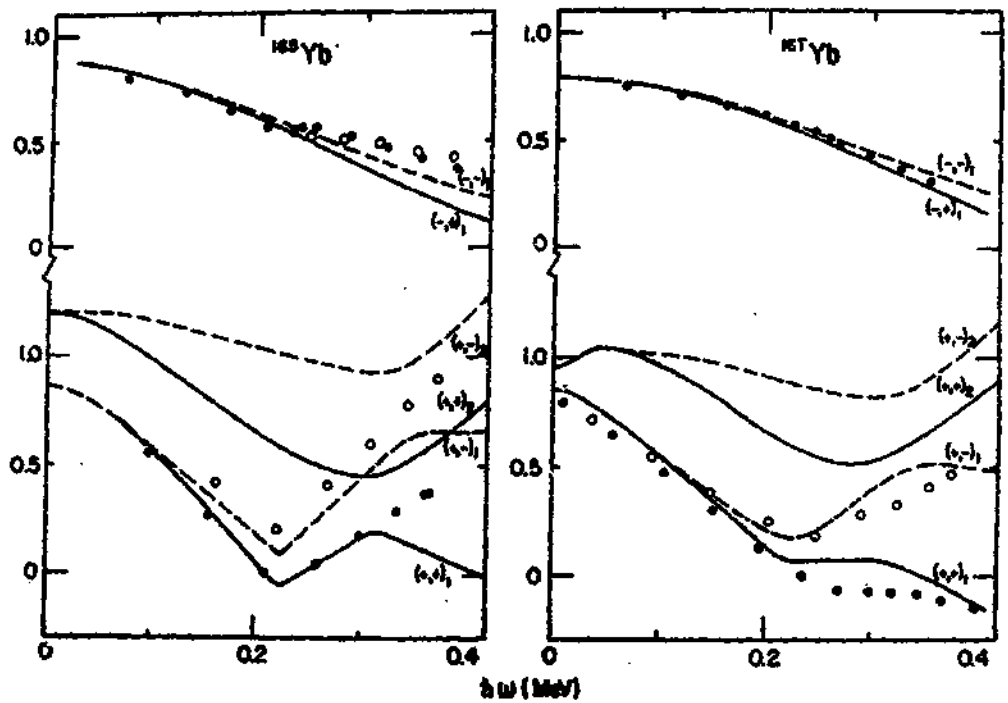

Fig. 20. Theoretical and experimental quasineutron spectra for ^{165}Yb and ^{167}Yb, shown as a function of $\hbar\omega$ and referred to an average of the yrast bands in ^{164}Yb and ^{166}Yb for ^{165}Yb and to the yrast band in ^{168}Yb for ^{167}Yb. The yrast references have been shifted in $\hbar\omega$ so as to make the crossing frequencies of the references coincide with the lowest-frequency crossings in the negative parity bands in ^{165,167}Yb. The open and the closed circles represent the experimental spectra for the negative and the positive signatures, respectively. The quantuum numbers appropriate for the theoretical spectra are also shown in the figure.

In fact, it has been suggested [18] that such an approach may be better, since the interaction at a crossing is never zero and at the large angular frequencies the spectrum of quasiparticle level becomes complicated. Several practical problems, however, are encountered in referring the odd-N experimental routhians to the yrast bands of the neighbouring even-even isotopes. Ideally, the average routhian of the yrast line from the even-even isotopes with one less and one more neutron can be constructed as a function of $\hbar\omega$ and substracted as a reference from the odd-N isotope of interest. It is known, however, that the frequency for the alignment of the first pair of $i_{13/2}$ neutrons is different in odd-N and even-N isotopes [25]. Therefore, it is necessary to shift the reference or the experimental vacuum in $\hbar\omega$ so that the crossing frequency of the reference coincides with that in the isotope of interest. Besides the shift in the alignment frequency for the first pair of $i_{13/2}$ neutrons, a shift in the magnitude of the alignment associated with this pair of neutrons is apparently observed between the two-quasineutron and three-quasineutron configurations, resulting presumably from the reduced pairing caused by the larger number of aligned quasiparticles. Another problem, which must be considered when applying the experimental yrast line as a reference to the neighbouring isotope, is the variation between neighbouring isotopes of the interaction betwee the constituent bands of the yrast configuration [23,46,49]. The appropriate treatment for such change in the alignment and in the interband interaction strength between the neighbouring even- and odd-N isotopes is not a priori obvious. Therefore, the approach is to examine for ^{165}Yb the comparison between the experimental and predicted routhians for both reference frames and then to consider ^{167}Yb where only the reference to the yrast band is appropriate.

When the experimental routhians of ^{165,167}Yb are referred to the yrast configuration, the crossing in the negative-parity bands should disappear (compare figs. 19 and 20). Therefore, the extent to which this band crossing is removed is a test of whether an appropriate reference has been chosen. In the yrast representa-

tion configurations are labelled by the non-yrast excited quasiparticles. For example, the ground-state bands of ^{165,167}Yb will be $(-,+)_1$ at $\hbar\omega$ below as well as above the band crossing, since the $i_{13/2}$ neutrons are also aligned in the reference. The discontinuity in the experimental routhian of the $(-,+)_1$ band of the ^{165}Yb (see fig. 20) at the crossing and the change of slope of the routhian at this point are associated with reference problems. The pairing correlations and interband interactions in the yrast bands of ^{164,166}Yb are not completly applicable to ^{165}Yb.

The ^{167}Yb experimental routhians, shown in fig. 20, are referred to the yrast band of ^{168}Yb [50,51]. A constant value of E_ν= 0.79 MeV has been included in the routhian. This value corresponds to Δ_n = 0.745 MeV plus a contribution from $\epsilon_\nu - \lambda$, which accounts for the fact that the Fermi surface in ^{167}Yb is located in a gap between $5/2^-[523]$ and $7/2^+[633]$ levels in the Nilsson scheme (see fig. 10). Had the yrast band, with its weak ground-state band s-band interaction, been used as a reference for ^{167}Yb, with its strong interaction between the ground-state band and its crossing band, a very pronounced discontinuity would have been produced in the negative-parity band at the crossing frequency. Similarly, the large s-band alignment in ^{166}Yb would have led to a slope change in the ^{167}Yb negative-parity band above the band crossing frequency. The routhians of the positive-parity bands of ^{167}Yb are at low $\hbar\omega$, lower in excitation energy than predicted, indicating either that the predicted energy separation between the $5/2^-[523]$ and the $5/2^+[642]$ Nilsson configurations is too large or that the Fermi surface should be closer to the $7/2^+[633]$ Nilsson state than to the $5/2^+[642]$ state (see fig. 10). Similar to ^{161,163,165}Yb and other odd-N rare-earth nuclei [10] the signature splitting between the $(+,+)_1$ and the $(+,-)_1$ configurations is observed to be larger than predicted. In contrary to the case of ^{165}Yb, the crossing in the $(+,+)_1$ band, corresponding to the alignment of the second combination of $i_{13/2}$ neutrons (i.e. the exchange of character of the $(+,+)_1$ and the $(+,+)_2$ configurations) is close to the predicted frequency. This crossing, which corresponds to the change in the slope of the $(+,+)_1$ routhian at

$\hbar\omega \approx 0.32$, is characteristic of strongly interacting configurations in agreement with the calculations. The band crossing in the $(+,-)_1$ band, corresponding to an exchange in character of the $(+,-)_1$ and $(+,-)_2$ configurations, is not observed up to $\hbar\omega \approx 0.375$ MeV, whereas it is predicted at a lower angular frequency (see fig. 20). For the lighter Yb isotopes, the crossings of the $(+,+)_1$ and $(+,-)_1$ bands are found at nearly equal frequencies [52]. This feature is connected probably with the low-Ω components (having thus large alignment) which mixe into the $(+,+)_1$ quasineutron for $N \geqslant 95$, thereby depressing the $(+,+)_2$ trajectory with respect to the $(+,-)_2$ one (see fig. 18). For the lower-mass Yb isotopes, the highly aligned low-Ω trajectories are close to the Fermi surface and therefore are the dominant components of those quasineutron configurations.

9. Evidence for strong rotational effects on M1 transitions.

The interband M1 transitions matrix elements connecting states in rotational bands based on the opposite signatures of high-j, low-Ω quasiparticle orbits are predicted [53] to be strongly signature dependent even for small rotational frequencies. The M1 transitions between bands based on the $(+,+)_1$ and $(+,-)_1$ configurations in light odd-N Yb should provide an excellent test of these predictions, since these bands are strongly populated in (H.I., xn) reactions. In fact, such transitions in ^{161}Yb [21,24] were used as the original examples of this effect. The interband transitions between the $(+,+)_1$ and $(+,-)_1$ bands in ^{163,165,167}Yb provide an even more sensitive test of the signature-dependent rotational effect on the M1 transitions. Not only are more transitions observed in ^{163,165,167}Yb than in ^{161}Yb, but in ^{165}Yb the signature splitting in energy is such that the I-1 state in the $(+,-)_1$ band is nearly degenerated with the I state in the $(+,+)_1$ band (see fig. 3). This is exactly the condition for the M1 matrix elements of the $(I+1, \alpha=-1/2 \rightarrow I, \alpha=1/2)$ transitions to approach zero, and for the $(I, \alpha=1/2 \rightarrow I-1, \alpha=-1/2)$ transitions to have the maximum enhancement [53]. For example, $B(M1, 23/2^+ \rightarrow 21/2^+)$ should be very small and $B(M1, 21/2^+ \rightarrow 19/2^+)$ is expected to be large. In ^{165}Yb, the γ-ray energies of the $(I, \alpha=1/2 \rightarrow I-1, \alpha=-1/2)$ transitions in the yrast band are so small that these transitions cannot compete with the strongly-enhanced $(I \rightarrow I-2)$ transitions along the yrast band. The $(I+1, \alpha=-1/2 \rightarrow I, \alpha=1/2)$ transitions, which should be greatly hindered are observed. In ^{163}Yb and ^{167}Yb, where the signature splitting is smaller, both types of M1 transitions between the positive-parity bands appear.

Although no absolute transition rates have been measured, some information on the M1 matrix elements can be extracted by a comparison with the E2 strength which is assumed to follow the pattern of the rigid rotation. Rotational perturbations on B(E2) values for the $(I \rightarrow I-1)$ transitions between the signature partners and for in-band $(I \rightarrow I-2)$ transitions are expected to be very

small [53]. From the experimental branching ratios $\lambda = \Gamma(I \to I-2) / \Gamma(I \to I-1)$, a value of

$$\frac{B(M1)}{Q_0^2} = \frac{E_{\gamma 1}^2}{14.41} \cdot \left[\left(\frac{E_{\gamma 2}}{E_{\gamma 1}} \right)^5 \cdot \langle IK\ 20/I-2K \rangle^2 \cdot \frac{1}{\lambda} - \langle IK\ 20/I-1K \rangle^2 \right] \qquad /12/$$

can be evaluated. It is also possible to use the experimental values of the mixing ratios δ within the $I \to I-1$ transitions to determine the same ratio.

$$\frac{B(M1)}{Q_0^2} = \frac{E_{\gamma 1}^2}{14.41} \cdot \frac{\langle IK20/I-1K \rangle^2}{\delta^2} \qquad /13/$$

In both expressions $E_{\gamma 1}$ and $E_{\gamma 2}$ correspond to the energies in keV fo $I \to I-1$ and the $I \to I-2$ transitions, respectively. The data presented in fig. 21 have been derived, assuming a value of $Q_0 = 7$ eb. For all nuclei studied, $K = 5/2$ was used to get the values of $\frac{B(M1)}{Q_0^2}$. Since the rotation is expected to mix lower K values into the wave function, values of $K = 3/2$ and $1/2$ were also applied and were found to increase $B(M1)$'s extracted from the branching ratio λ, while the $B(M1)$ values obtained from the mixing ratio δ were found to decrease drastically. The experimental determination of δ involves a larger uncertainty than that of the λ-value but, in order to bring the two extracted values of $B(M1)$ into agreement the average value of K has to be shifted of about 1/2 unit below 5/2. The values presented in fig. 21 have been derive from the branching ratios with this K-admixture taken into account. The effect is found to be the largest on the highly retarded $B(M1)$ values in ^{161,163,165}Yb. For ^{167}Yb, the separation between the $B(M1)$ values for the transitions between the two signatures is observed, but in this nucleus the retardation is less pronounced, as is expected, since the Fermi surface lies here further away from the low-Ω orbits of the $i_{13/2}$ configuratic

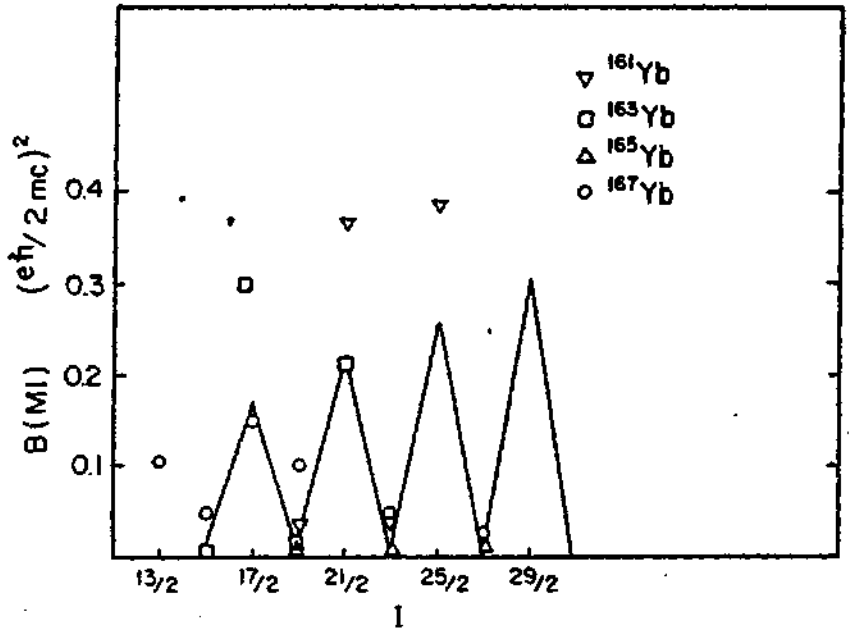

Fig. 21. B(M1) values for I→I-1 transitions between states of opposite signature of the $i_{13/2}$ band in odd-A Yb nuclei. These values were derived using Q_0^2 = 50 $e^2.b^2$ and the average value K = 2 (see text). The zigzag line shows the theoretical values appropriate for the ^{165}Yb, calculated from the particle-rotor model [53].

Since the 1/2 [660] is closer to the Fermi surface in ^{161}Yb and ^{163}Yb than in ^{165}Yb for which the calculation is performed, a larger signature dependence is observed for the two lighter Yb nuclei.

10. Summary

The studies on which this paper is based can be regarded as a test case for the cranked shell-model in a region of nuclei with stable deformation. Routhians and alignments have been extracted from the experimental data. Experimental single-quasineutron routhians have been used to construct two- and three-quasineutron routhians. The $\hbar\omega$ and configuration dependences of the constructed routhians for two-quasineutron configurations in ^{162,164,166}Yb agree with the experimental data, suggesting that the residual interaction between two unpaired quasineutrons is only weakly dependent upon the configurations and frequency. A comparison of the magnitude of the neutron pairing-correlation parameter obtained from the energy difference between the two-quasineutrons routhians and the sum of the constituent single-quasineutron routhians with the neutron odd-even mass difference, and the pairing-correlation parameter obtained from the $\hbar\omega_c$ of the band crossing in the ^{166}Yb yrast sequence gives a residual interaction of about 300 keV between the unpaired quasineutrons.

An empirical odd-even neutron-number dependence of the rotational frequency for the alignment of the first pair of $i_{13/2}$ quasineutrons has been established. This behaviour is explained by a reduction of Δ_n for odd-N systems as compared to the seniority-zero neutron configurations in even-N nuclei. A comparison of the magnitudes of the Δ_n^{CSM} necessary to reproduce the crossing frequencies with Δ_n^{oe} (from odd-even mass difference) indicates that it may be possible to obtain quantitative values of Δ from the crossing frequencies of quasipartiole bands. The agreement between Δ_n^{CSM} and Δ_n^{oe} indicates also that Δ_n is not strongly dependent upon $\hbar\omega$ for values of $\hbar\omega < \hbar\omega_c$. The loss in neutron pairing is associated apparently with neutron alignment and independent of proton alignment.

Finally, it has been shown, that it is possible to make a direct comparison between calculated quasiparticle energies for independent particle motion in a rotating deformed nucleus and high-spin decay-scheme data expressed in the e' versus $\hbar\omega$ repre-

sentation. Such a comparison has been made for a large number of quasineutron configurations in rare-earth nuclei of varying neutron number. The agreement is surprisingly good despite the simple assumptions of the cranked shell model (all parameters, ε_2, ε_4, Δ_n, K, μ, λ independent of $\hbar\omega$). However several problems are not solved yet:

1/ It is necessary to reduce Δ_n for configurations with a larger number of excited quasineutrons.

2/ The predicted signature splitting is too large for the lowest negative-parity levels near N=91.

3/ It is difficult to reproduce simultaneously the signature splitting in the positive-parity band and the band-crossing frequencies near N=95.

The drastic effect of rotation on M1 transition matrix elements between the nucleons in high-j orbits has also been observed in agreement with the calculations of I. Hamamoto.

Acknowledgements

I am very grateful to Prof. Prof. A.Z. Hrynkiewicz, S. Ogaza and A. Strzałkowski for their stimulating interest during my work.

The studies discussed in this paper would not have been possible without a fruitful and vigorous collaboration between theoreticians and experimentalists. I want to express my sincere gratitude to all my collaborators from different laboratories, who have taken part in those studies, for fruitful discussions, a pleasant and inspiring collaboration. In particular thanks are due to Prof. Prof. Hans Ryde, J.D. Garrett, G.B. Hagemann and B. Herskind.

I wish to express my sincere thank to the Swedish Natural Science Research Council for financial support during my stay at the Lund University.

Finally, I would like to thank my colleagues from the Institute of Nuclear Physics, the Jagellonian University and the Lund University for their continuous help.

References

1. S. Cohen, P. Plasil and W.J. Świątecki, Annals of Physics 82, 557 (1974)
2. J.R. Grover, Phys. Rev. 157, 832 (1967)
3. A. Bohr and B.R. Mottelson, Physica Scripta 10A, 13 (1974)
4. A. Bohr and B.R. Mottelson, J. Phys. Soc. Japan 44, 157 (1978)
5. F.S. Stephens and R.S. Simon, Nucl. Phys. A183, 257 (1972)
6. A. Bohr and B.R. Mottelson, Mat. Fys. Medd. Dan. Vid. Selsk. 27, No 16 (1953)
7. A.K. Kerman, Mat. Fys. Medd. Dan. Vid. Selsk. 30, No 15 (1956)
8. A. Bohr, B.R. Mottelson, Nuclear Structure Vol. II, W.A. Benjamin Inc. (1975)
9. D.R. Inglis, Phys. Rev. 96, 1059 (1954)
10. R. Bengtsson and S. Frauendorf, Nucl. Phys. A314, 27 (1979); R. Bengtsson and S. Frauendorf, Nucl. Phys. A327, 139 (1979)
11. W. Waluś, N. Roy, S. Jönsson, L. Carlén, H. Ryde, G.B. Hagemann, B. Herskind, J.D. Garrett, Y.S. Chen, J. Almberger and G. Leander, Physica Scripta 24, 324 (1981)
12. N. Roy, S. Jönsson, H. Ryde, W. Waluś, JJ. Gaardhøje, J.D. Garrett, G.B. Hagemann and B. Herskind, University of Lund, Report LUIP 8107, Lund 1981; Nucl. Phys. A382, 125 (1982)
13. J. Kownacki, J.D. Garrett, G.B. Hagemann, B. Herskind, W. Waluś, N. Roy, S. Jönsson, L. Carlén, H. Ryde, Verhandl. DPG 4, 728 (1981)
14. J. Kownacki, J.D. Garrett, J.J. Gaardhøje, G.B. Hagemann, B Herskind, S. Jönsson, N. Roy, H. Ryde and W. Waluś, NBI preprint 1982 ; submitted for publication in Nucl. Phys. A
15. L. Carlén, S. Jönsson, J. Krumlinde, J. Lyttkans, N. Roy, H. Ryde, S. Strömberg, W. Waluś, G.B Hagemann and B. Herskind, University of Lund, Report LUIP 8109, Lund 1981; Nucl. Phys. A381, 155 (1982)
16. G.B. Hagemann, R. Broda, B. Herskind, M. Ishihara, S. Ogaza and H. Ryde, Nucl. Phys. A245, 166 (1975)
17. P.O. Tjøm, I. Espe, G.B. Hagemann, B. Herskind and D.L. Hillis, Phys. Lett. 72B, 439 (1978)
18. I. Hamamoto, NORDITA preprint 81/28, Copenhagen, 1981
19. M.A.J. Mariscotti, G. Scharff-Goldhaber, B. Buck, Phys. Rev. 178, 1864 (1969)
20. L.M. Harris, Phys. Rev. 138B, 509 (1965)
21. L.L. Riedinger, O. Andersen, S. Frauendorf, J.D. Garrett, J.J. Gaardhøje, G.B. Hagemann, B. Herskind, Y.V. Makovetzky, J.C. Waddington, M. Guttormsen and P.O. Tjøm, Phys. Rev. Lett. 44, 568 (1980); and to be published
22. J.D. Garrett and J.J. Gaardhøje, in Proc. XIV Summer School on Nuclear Physics, Mikołajki, Poland, Aug.31 - Sept.12, 1981, Nukleonika, in press.
23. S. Frauendorf, Physica Scripta 24, 349 (1981)
24. J.J. Gaardhøje, thesis, University of Copenhagen, 1980
25. J.D. Garrett, O. Andersen, J.J. Gaardhøje, G.B. Hagemann, B. Herskind, J. Kownacki, J.C. Lisle, L.L. Riedinger, W. Waluś, N. Roy, S. Jönsson, H. Ryde, M. Guttormsen and P.O. Tjøm, Phys. Rev. Lett. 47,75 (1981)

26. F.A. Beck, E. Bożek, T. Byrski, C. Gehringer, J.C. Merdinger, Y. Schulz, J Styczeń, J P Vivien, Phys. Rev. Lett. 42, 492 (1979)
27. L.L. Riedinger, W.K. Luk, D.R. Haenni, S.A. Hjorth, N.R. Johnson, I.Y. Lee, R.L. Robinson, in Proc. Int. Conf. on nuclear physics, Berkeley, (1980) Vol. 1, p. 383; L.L. Riedinger, Physica Scripta 24, 312 (1981)
28. I.Y. Lee, M.M. Aleonard, M.A. Deleplanque, Y. El-Masri, J.O Newton, R.S. Simon, R.M. Diamond and F.S Stephens, Phys. Rev. Lett. 38, 1454 (1977)
29. J. Simpson, P. Smith, J. Sharpey-Schafer, P. Butler, J.D. Garrett, G.B. Hagemann, B. Herskind, to be published
30. H. Ryde, S.A. Hjorth, D. Barheoud, A. Johnson, G.B. Hagemann, B. Herskind, Nucl. Phys. A207, 513 (1973)
31. O.C. Kistner, A.W. Sunyar, E. der Mateosian, Phys. Rev. C17, 1417 (1978)
32. A. Johnson, H. Ryde, S.A. Hjorth, Nucl. Phys. A179, 753 (1972)
33. J. Bacelar, R. Chapman, J.C. Lisle, J.N. Mo, A. Simcock, J.C. Willmott, J.D. Garrett, G.B. Hagemann, B. Herskind, to be published
34. L.L. Riedinger, Physica Scripta 24, 312 (1981)
35. I. Rezanka, I.M. Ladenbauer-Bellis, J.O. Rasmussen, W. Ribbe, E. der Mateosian, Phys. Rev. C11, 1767 (1975)
36. J.C. Lisle, J.D. Garrott, G.B. Hagemann, B. Herskind, S. Ogaza, Nucl. Phys. A366, 281 (1981)
37. G.D. Dracoulis, P.M. Walker, Nucl. Phys. A339, 186 (1979)
38. R.V.F. Janssens, M.J.A. de Voigt, H. Sakai, H.J.M. Aarts, C.J. Van der Poel, H.F.R. Arciszewski, D.E.C. Scherpenzeel and J. Vervier, KVI preprint, KVI-308 1981
39. G.D. Dracoulis, P.M. Walker, A. Johnston, J. Phys. G4, 713 (1978)
40. P.M. Walker, G.D. Dracoulis, A. Johnston, J.R. Leigh, M.G. Slocombe, I.F. Wright, J. Phys. G4, 1655 (1978)
41. J.D. Garrett, G.B. Hagemann, B. Herskind, G. Sletten, G. Løvhøiden, T.F. Thowsteinsen, A. Henriques, F. Ingebretsan, J. Rekstad, P.O. Tjøm, NBI preprint (1981)
42. A.J. Larabee, J. Waddington, McMaster University preprint (1981)
43. E.R. Marshalek and A.L. Goodman, Nucl. Phys. A294, 92 (1978); A.L. Goodman, Phys. Rev. Lett. 42, 357 (1979)
44. A.H. Wabstra, K. Bok, Nucl. Data Tables 19, 175 (1977)
45. G. Andersson, S.E. Larsson, G. Leander, P. Möller, S.G. Nilsson, I. Ragnarsson, S. Åberg, R. Bengtsson, J. Dudek, B. Nerlo-Pomorska, K. Pomorski and Z. Szymański, Nucl. Phys A268, 205 (1976)
46. R. Bengtsson, J.de Physique (colloque) C10, 84 (1980)
47. R. Bengtsson, H.B. Håkansson, Nucl. Phys. A357, 61 (1981)
48. R. Bengtsson and J-y. Zhang, in Proc. of nucl. physics Workshop, Trieste, Oct. 5-10, 1981, to be published
49. R. Bengtsson, I. Hamamoto, B. Mottelson, Phys. Lett. 73B, 259 (1978)
50. O.C. Kistner et al., private communication.
51. I. Hamamoto, Phys. Lett, 102B, 225 (1981); and I. Hamamoto, NORDITA preprint 81/39

52. L.L. Riedinger, Nucl. Phys. A347, 141 (1980)
53. I. Hamamoto, Phys. Lett. 106B, 281 (1981); and I. Hamamoto, Phys. Lett. 102B, 225 (1981)